Charles University in Prague

Faculty of Mathematics and Physics

DIPLOMA THESIS

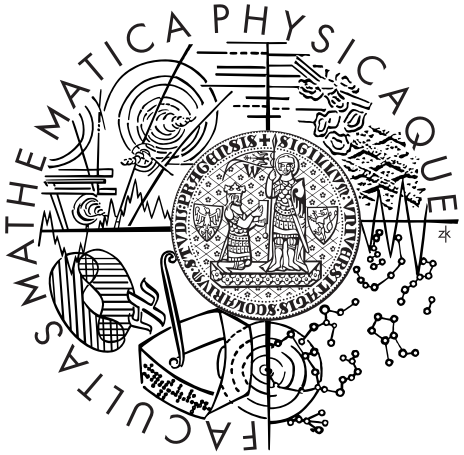

Daniel Červenkov

Studium procesů s účastí kvarku b v experimentu Belle

Study of b-quark processes in the Belle experiment

Institute of Particle and Nuclear Physics

Supervisor: Zdeněk Doležal

Co-Supervisor: Karim Trabelsi

Study programme: Physics

Study branch: Nuclear and Sub-Nuclear Physics

Prague 2012

I would like to express gratitude to Karim Trabelsi for supervising this thesis and for his insightful comments and ideas. I would also like to thank Zdeněk Doležal for supervising this thesis and giving me the opportunity to work on this topic. My gratitude goes to Zbyňek Drásal as well, for the physics and analysis discussions we had. Last but not least I would like to thank my family for their lifelong support and even editing assistance, and most of all Eliška for enjoying life together with me.

Prohlašuji, že jsem tuto diplomovou práci vypracoval samostatně a výhradně s použitím citovaných pramenů, literatury a dalších odborných zdrojů.

Beru na vědomí, že se na moji práci vztahují práva a povinnosti vyplývající ze zákona č. 121/2000 Sb., autorského zákona v platném znění, zejména skutečnost, že Univerzita Karlova v Praze má právo na uzavření licenční smlouvy o užití této práce jako školního díla podle §60 odst. 1 autorského zákona.

I declare that I wrote this diploma thesis independently and exclusively with the use of the cited sources. I agree with lending the thesis.

Prague, August 3, 2012 Daniel Červenkov

Název práce: Studium procesů s účastí kvarku b v experimentu Belle

Autor: Daniel Červenkov

Katedra: Ústav jaderné a subjaderné fyziky

Vedoucí diplomové práce: Doc. RNDr. Zdeněk Doležal, Dr.

Konzultant: Dr. Karim Trabelsi

Abstrakt: Byla provedena studie zabývající se proveditelností měření $\sin(2\phi_1+\phi_3)$ s využitím rozpadového kanálu $B^0 \to D^{*\mp}\rho^{\pm}$ a dat experimentu Belle. Vytvořili jsme dva fittery. Časově nezávislý, který vykazuje vysokou stabilitu a vrací velmi uspokojivé statistické chyby a časově závislý. Při testování druhého fitteru, jsme objevili chybu v EvtGen a navrhli dočasné řešení. Přesto časově závislý fitter nenachází správné hodnoty. K dosažení rozhodných výsledků bude zapotřebí další práce.

Klíčová slova: B meson, úhlová analýza, časová závislost, fitter

---

Title: Study of b-quark processes in the Belle experiment

Author: Daniel Červenkov

Department: Institute of Particle and Nuclear Physics

Supervisor: Zdeněk Doležal

Co-Supervisor: Karim Trabelsi

Abstract: A study regarding the plausability of using the $B^0 \to D^{*\mp}\rho^{\pm}$ decay channel and the data set of the Belle experiment to measure $\sin(2\phi_1+\phi_3)$ has been carried out. Two fitters have been created. A time-independent one, which exhibits high stability and reports gratifying fit uncertainties, and a time-dependent one. During the testing of the latter we have discovered an EvtGen flaw and proposed a temporary workaround. Nevertheless, the time-dependent fitter fails to recover the correct values. More work will be needed to reach conclusive results.

Keywords: B meson, angular analysis, time-dependent, fitter

Contents

Introduction

Symmetries have fascinated mankind from times immemorial. They manifest themselves in most diverse forms, in a score of fields and across all scales, from the cosmological to that of elementary particles. Some symmetries seem to be perfect, while others are slightly broken.

This work is dedicated to one of the near-symmetries of the universe and its breaking. One that 'acts' on the very small scales, but has extremely serious repercussions for the whole universe - the charge-parity (CP) symmetry. It is a product of two distinct symmetries: the charge conjugation (C) - exchanging particles for their antiparticles, and parity (P), which creates a mirror image of a physical system. If it were a perfect symmetry the world would look very different than it does today. Mainly because there would be almost no matter present in it, just a sea of radiation from particles and antiparticles that mostly annihilated each other shortly after the Big Bang.

There are only two mechanisms in the Standard Model that can break CP symmetry. One involves the Quantum Chromodynamic Lagrangian, thus breaking the CP symmetry of the strong force, for which there have been no experimental indications as of yet. The second is connected to the weak force and breaks CP symmetry through a single non-trivial complex phase in the Cabibbo-Kobayashi-Maskawa quark mixing matrix. Some of the properties of this matrix can be expressed in terms of 'unitarity triangles' as discussed later, in Chapter 3. The existence of this second mechanism is now well established and physicists are working hard to constrain its parameters.

This thesis studies the plausibility of exploiting the $B^0 \to D^{*\mp}\rho^{\pm}$ process using data collected by the Belle experiment ($\sim 1\,\mathrm{ab}^{-1}$) and/or potentially Belle II, to further constrain some of the parameters of the Standard Model, including the mentioned unitarity triangles.

Chapter 1

Historical background

Until the year 1956 it was widely believed in the physics community that the laws of nature are invariant under the parity transformation ($\vec{x} \to -\vec{x}$). It was then that the theoretical physicists T. D. Lee and C. N. Yang pointed out, in a carefully written article [1], that this assumption was never verified for weak interactions. During that same year the group of C.-S. Wu carried out the famous experiment [2] that found a violation of parity symmetry in beta decay of cobalt-60. Consequently, in 1957, T. D. Lee and C. N. Yang were awarded the Nobel Prize "for their penetrating investigation of the so-called parity laws which has led to important discoveries regarding the elementary particles" [3].

In 1957 L. Landau proposed [4] that combined charge-parity might be an exact symmetry. That idea lasted a bit longer, but it was eventually disproved as well, in 1964 by J. W. Cronin and V. L. Fitch et al., by finding CP violation in the decay of neutral kaons [5]. This discovery resulted in a Nobel Prize for the two in 1980.

It took almost half a century before CP violation was observed outside the kaon system. This was achieved in 2001 by the Belle collaboration, in the B meson system. Since then, many CP violating processes in B decays have been discovered.

More recently, in 2011, the LHCb experiment in CERN reported the first indication of CP violation in decays of neutral D mesons [6].

Chapter 2

Belle Experiment

The Belle experiment is a collaboration of more than 350 physicists and engineers from 68 institutes in 16 countries [7]. The research is centered around data collected by the Belle detector located at the interaction point of the KEKB accelerator at the High Energy Accelerator Research Organization (KEK) in the city of Tsukuba in Japan.

Belle, as well as its sister experiment BaBar in SLAC in California, was designed and built with a very specific purpose in mind: to test the Cabibbo-Kobayashi-Maskawa description of quark mixing and CP violation in the Standard Model of particle physics. The goals of testing this part of the Standard Model were achieved, and have been surpassed beyond all expectations.

However, the precision of the Belle detector also allows for many other scientific searches, such as those for rare decays, exotic particles, dark matter, as well as precision measurements of the properties relating to B mesons, D mesons and taus.

Extensive studies of these subjects resulted in more than 300 publications in various physics journals. Among the collaboration's achievements are the first observation of CP violation in the B system in 2001 and discovery of a multitude of new particles including such exotics as $X(3872)$. Last but not least the insight into CP violation the Belle experiment brought lead into a Nobel prize for M. Kobayashi and T. Maskawa in 2008.

The Belle experiment, after gathering data for over a decade, finished operation in mid-2010. An upgrade of both the accelerator and the detector is underway announcing a new generation of B-factories.

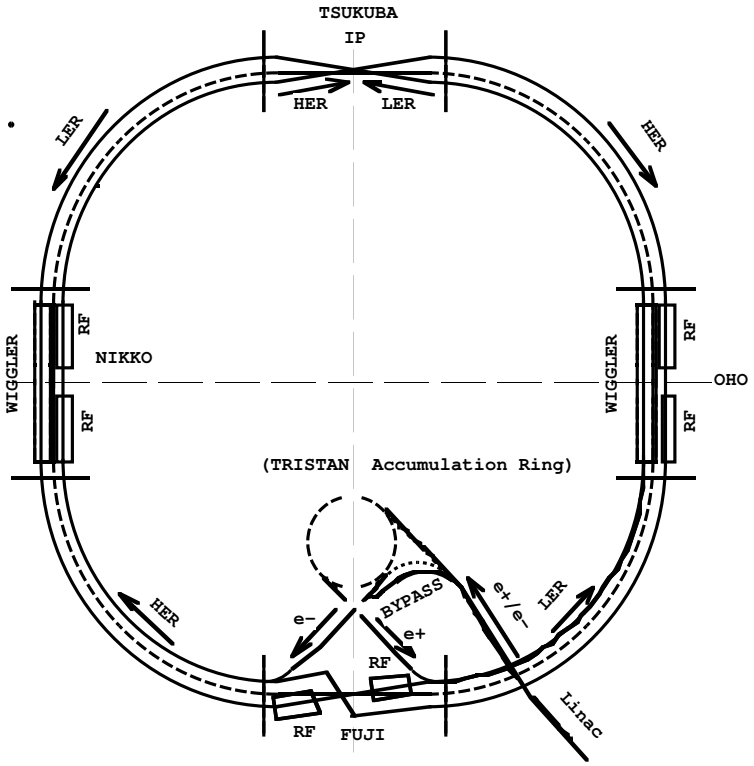

Figure 2.1: The KEKB Accelerator

2.1 KEKB Accelerator

The KEKB was an asymmetric electron-positron collider. Most of its operational time it run at the center-of-mass energy $\sqrt{s} = 10.58\,\mathrm{GeV}$ which is equal to the rest mass of the $\Upsilon(4S)$ resonance, i.e., a bound state of $b\bar{b}$ quarks, that has just high enough mass, that in 96% it decays to either B^+B^- or $B^0\bar{B}^0$ [8]. This choice of center-of-mass energy along with optimizations for increasing luminosity (KEKB holds the world record for the highest luminosity machine, having achieved $\mathcal{L} = 2.11 \times 10^{34}\,\mathrm{cm}^{-2}\mathrm{s}^{-1}$ [9]), lead to the production of a copious amount of B mesons. Because of this such colliders are usually called B-factories, although large numbers of D mesons and taus are produced there as well. The KEKB accelerator had basically two separate rings: a High Energy Ring (HER) for electrons having 8 GeV and a Low Energy Ring (LER) for positrons at 3.5 GeV. Both rings resided side by side in the accelerator tunnel, which was excavated for the prior accelerator TRISTAN. The circumference of each ring was 3016 m [9] and they were composed of four straight sections and four bends as depicted in Fig. 2.1.

The asymmetry in beam energies is characteristic of B-factories. It provides a

Lorentz boost to the produced $\Upsilon(4S)$ resonance and consecutively the B mesons. This allows for a precise measurement of their decay times because of time dilatation. It is straightforward to calculate how much this boost helps. Please note that throughout this text the natural unit convention will be used ($\hbar = c = 1$).

Let us assume that the particle beams are collinear (neglecting the 11 mrad angle between them) and, in accordance with the Belle convention, are parallel to the z axis.

Relativistic momentum is defined as

$$\vec{p} = \gamma m_0 \vec{\beta}. \tag{2.1}$$

Taking into account that in our case $\vec{p} = (0, 0, p)$ and $\vec{\beta} = (0, 0, \beta)$ we get

$$\beta\gamma = \frac{p}{m_0}. \tag{2.2}$$

Now we have to be mindful of what the p and m_0 in the previous equation stand for. We are interested in the Lorentz boost of the system resulting from the collision of e^+ and e^- with respect to the laboratory frame. Therefore the mass parameter m_0 has to be the *invariant* mass of the e^+e^- system and p is its momentum, which is simply a vector sum of the momenta of both particles. As we can safely neglect the electron mass with respect to its energy, we can write

$$p = |\vec{p}_1 + \vec{p}_2| = |(0, 0, 0, p_1 - p_2)| \doteq E_1 - E_2, \tag{2.3}$$

where we have designated the particle with higher energy, i.e., electron, as '1'. The invariant mass of two particles is $m_0 = \sqrt{s}$ where s is the well known Mandelstam invariant

$$s = (p_1 + p_2)^2 = (E_1 + E_2, \vec{p}_1 + \vec{p}_2)^2. \tag{2.4}$$

Using the Minkowski metric $\eta = \mathrm{diag}(1, -1, -1, -1)$ and neglecting electron mass we easily expand the previous result to

$$s = (E_1 + E_2)^2 - (\vec{p}_1 - \vec{p}_2)^2 \doteq 2E_1E_2(1 - \cos\theta) \tag{2.5}$$

In our case the electrons and positrons collide head-on, therefore $\theta = \pi$, leaving us with

$$s = 4E_1E_2. \tag{2.6}$$

Putting the previous equations together, along with $E_1 = 8\,\mathrm{GeV}$ and $E_2 = 3.5\,\mathrm{GeV}$ yields

$$\beta\gamma = \frac{p}{m_0} \doteq \frac{E_1 - E_2}{2\sqrt{E_1E_2}} \doteq 0.425 \tag{2.7}$$

The way the time between decays of the pair of B mesons is measured is indirect. In fact, the measured quantity is the distance between their decay vertices. The conversion of the distance to time is simple, once we have $\beta\gamma$, using

$$\Delta z = \beta\gamma\Delta t. \tag{2.8}$$

We see that the bigger $\beta\gamma$ is, the larger Δz becomes and thus it can be measured with higher relative precision.

2.2 Belle Detector

In this section we will provide only a brief overview of the Belle detector and its parts as this study was conducted on a generator level, and thus we did not have to consider such effects as a finite resolution, particle misidentification and other detector-specific intricacies.

The Belle detector was a 4π solid angle composite detector with rotational symmetry around the beam axis. It was, however, asymmetrical in the forward-backward direction due to the asymmetry of energy between the electron and positron beams. It consisted of the following sub-detectors, which are depicted in Fig. 2.2:

- SVD (Silicon Vertex Detector)

  The SVD was made of double-layer strip detectors, which enabled precise vertexing and tracking. This is especially important for time-dependent analyses, because the vertex positions are used to extract the time information.

- CDC (Central Drift Chamber)

  Another tracking sub-detector, one that exploits the 1.5 T magnetic field of a super-conducting solenoid, which resided between the electromagnetic calorimeter and the kaon/muon detector.

- ACC (Aerogel Cherenkov Counter)

  A threshold Cherenkov detector used in particle identification to separate kaons from pions.

- TOF (Time-of-flight counters)

  Another sub-detector used for particle identification.

- ECL (Electromagnetic Calorimeter) and EFC (Extremely Forward Calorimeter)

  A highly segmented CsI(Tl) calorimeter used for measuring the energy of electrons and photons via electromagnetic showers.

- KLM (Kaon Long/Muon detector)

  A detector that consisted of resistive plate counters interspersed in an iron yoke and was used to detect K_Ls and muons.

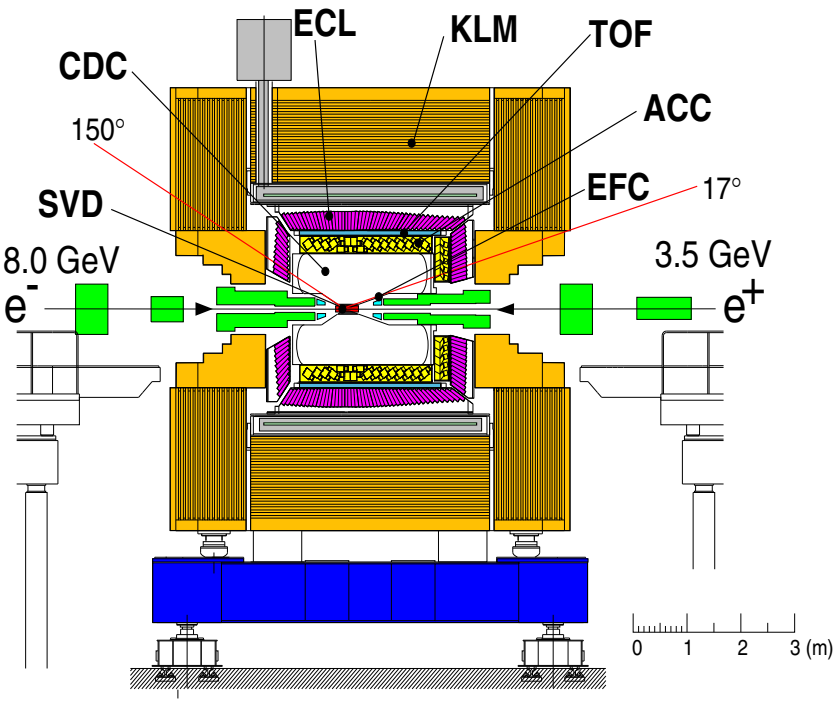

Figure 2.2: Side view of the Belle detector

All the sub-detectors combined were producing around 0.4 TB of raw data per day [10]. This beckoned for adequate data processing and storage systems, which were located on-site. It was a grid dedicated to the Belle experiment that used combined disk and tape storage.

The system went through an upgrade recently in anticipation of Belle 2. It is no longer dedicated to Belle, but is shared throughout KEK. Storage was vastly upgraded as the Belle 2 detector should acquire 50 times the Belle data amount by 2020 [11].

Chapter 3

Analysis

3.1 Helicity Basis

To study a decay process, one has to choose a suitable basis. For a decay of a scalar particle such as a B meson to two vector particles, e.g. D^* and ρ, helicity basis is very convenient.

Let us consider a general two-body decay of a particle with spin J, its projection along, e.g., z-axis of some arbitrary coordinate system being M. In the rest frame of the parent particle the daughters will have definite helicities λ_a and λ_b. The final state with a definite total angular momentum and definite helicities can be constructed as

$$|JM, \lambda_a \lambda_b\rangle = \mathcal{N} \int \mathrm{d}^3 n \, D^{J*}_{M,\lambda_a - \lambda_b}(\vec{n}) \, |\vec{n}, \lambda_a - \lambda_b\rangle, \tag{3.1}$$

where $\mathcal{N}$ is a normalization factor, $|\vec{n}, \lambda_a - \lambda_b\rangle$ is a two particle state with total angular momentum projection $\lambda_a - \lambda_b$ along the direction of the unit vector $\vec{n}$ and $D^{J*}_{M,\lambda_a-\lambda_b}(\vec{n})$ is the Wigner D-function. We exploited the fact, that in the rest frame of the parent particle the daughters have opposite momenta and therefore the total angular momentum of the system is the difference of their helicities.

In order to understand equation (3.1) we have to realize what the Wigner D-function represents. It is actually an element of a matrix in the irreducible representation of the group SO(3) also known as the rotational group in 3 dimen-

sional space. It is defined as [12]

$$D^J_{M,M'}(\vec{n}) \equiv D^J_{M,M'}(\phi,\theta,0) \equiv \langle JM|\hat{R}(\phi,\theta,0)|JM'\rangle, \tag{3.2}$$

where (ϕ,θ) are the polar coordinates of the vector $\vec{n}$ in the chosen basis and the rotation operator $\hat{R}$ is

$$\hat{R}(\phi,\theta,\psi) = e^{-i\phi\hat{J}_z}e^{-i\theta\hat{J}_y}e^{-i\psi\hat{J}_z}. \tag{3.3}$$

We can see that the complex conjugation of $D^J_{M,M'}(\vec{n})$ basically reverses the rotation. Therefore we can interpret $D^{J*}_{M,\lambda_a-\lambda_b}(\vec{n})$ as the probability amplitude to find within the state $|\vec{n},\lambda_a-\lambda_b\rangle$ a state with total angular momentum J and its projection M along the z-axis.

Consequently the construction of the state $|JM,\lambda_a-\lambda_b\rangle$ goes as follows: We integrate over all states of the final two particles (with correct total angular momentum/helicities, which has to be conserved of course) flying away in all possible directions modulated by the probability amplitude with which they contribute to the state with total angular momentum J and its projection M along the chosen axis.

The possible values of helicities are constrained by the relation

$$|\lambda_a - \lambda_b| \leq J, \tag{3.4}$$

which arises since the orbital angular momentum cannot have a component along the line of decay.

Now let us consider a more specific case of a scalar particle decaying to two vectors ones. We can write that down as

$$J = M = 0, \qquad s_a = s_b = 1. \tag{3.5}$$

Both daughter particles are in a spin triplet state and can therefore have helicities

$$\lambda_a, \lambda_b \in \{+1, 0, -1\}. \tag{3.6}$$

Combining equations (3.6) and (3.4) we get three possible combinations for the helicities of the two particles:

$$(\lambda_a, \lambda_b) \in \{(+1,+1),(0,0),(-1,-1)\}. \tag{3.7}$$

Obviously the final state can then be written as

$$|\Psi_f\rangle = \sum_\lambda H_\lambda \, |f_\lambda\rangle, \qquad \lambda \in \{+1,0,-1\}, \tag{3.8}$$

where, for the sake of brevity, we have introduced

$$\begin{aligned} |f_{+1}\rangle &= |JM,+1+1\rangle, \\ |f_0\rangle &= |JM,00\rangle, \\ |f_{+1}\rangle &= |JM,-1-1\rangle. \end{aligned} \tag{3.9}$$

H_λ is the amplitude of the corresponding helicity state. We can express it as

$$H_\lambda = \langle f_\lambda | \hat{H} | B \rangle, \tag{3.10}$$

where $\hat{H}$ is the Hamiltonian responsible for the decay and $|B\rangle$ is the original scalar particle state.

Looking at equation (3.1), we see that from the decay of a scalar particle ($J = 0, M = 0$) we get $D^0_{0,0}(\vec{n})$. Taking into account equations (3.2) and (3.3) it is apparent that $D^0_{0,0}(\vec{n}) = 1$. That is to be expected since a scalar particle does not have any distinctive directions, hence the daughter particles must travel in all directions with the same probability.

We get an altogether different situation when the daughter vector particles a, b decay themselves, each into two new (scalar) particles

$$a \to a_1 + a_2, \qquad b \to b_1 + b_2. \tag{3.11}$$

Then we can employ equation (3.1) not only for the decay of the original scalar particle, but also for the decay of each of the vector daughters in their respective reference frames. Using $\int d^3n = \iint d\phi \, d\cos\theta$ (this is true because we consider

only $|\vec{n}| = 1$) we get

$$\begin{aligned}|B\rangle =& \mathcal{N} \sum_{\lambda} \iint \mathrm{d}\phi \, \mathrm{d}\cos\theta \, H_\lambda D^{0*}_{0,0}(\phi,\theta,0) \, |f_\lambda\rangle \\ =& \mathcal{N}' \sum_{\lambda} \iint \mathrm{d}\phi_a \, \mathrm{d}\cos\theta_a \iint \mathrm{d}\phi_b \, \mathrm{d}\cos\theta_b \times \\ & \times H_\lambda \, D^{s_a *}_{\lambda,\lambda_{a_1}-\lambda_{a_2}}(\phi_a,\theta_a,0) \, D^{s_b *}_{\lambda,\lambda_{b_1}-\lambda_{b_2}}(\phi_b,\theta_b,0) \times \\ & \times |\vec{n}_a,\lambda_{a_1}\rangle| - \vec{n}_a,\lambda_{a_2}\rangle |\vec{n}_b,\lambda_{b_1}\rangle| - \vec{n}_b,\lambda_{b_2}\rangle.\end{aligned} \tag{3.12}$$

We can conclude that the amplitude for a decay of a scalar particle to two vector particles a and b which in turn decay to two new particles each, (a_1, a_2) and (b_1, b_2), a_1 traveling in the direction (ϕ_a, θ_a) and b_1 in (ϕ_b, θ_b) in the rest frames of their respective parent particles, is the following (up to a numerical factor)

$$A = \sum_{\lambda} H_\lambda \, D^{s_a *}_{\lambda,\lambda_{a_1}-\lambda_{a_2}}(\phi_a,\theta_a,0) \, D^{s_b *}_{\lambda,\lambda_{b_1}-\lambda_{b_2}}(\phi_b,\theta_b,0). \tag{3.13}$$

The z-axis of the rest frame of a is taken to be in the direction of its momentum $\vec{p}$ in the rest frame of the original, scalar, particle. Similarly, the z-axis in the rest frame of b is taken in the direction of *its* momentum in the original frame, i.e., $-\vec{p}$.

Looking closely at the definitions of D-functions and rotations one might notice how to simplify the preceding expression. Combining (3.2) with (3.3) yields

$$D^J_{M,M'}(\phi,\theta,\psi) = \langle JM | e^{-i\phi\hat{J}_z} e^{-i\theta\hat{J}_y} e^{-i\psi\hat{J}_z} | JM' \rangle. \tag{3.14}$$

Both states $|JM\rangle$ and $|JM'\rangle$ are eigenstates of $\hat{J}_z$ with eigenvalues M, M' respectively, therefore

$$e^{-i\psi\hat{J}_z}|JM\rangle = e^{-i\psi M}|JM\rangle. \tag{3.15}$$

We can define a Wigner d-function by the relation

$$D^J_{M,M'}(\phi,\theta,\psi) = e^{-i\phi M} e^{-i\psi M'} \langle JM | e^{-i\theta\hat{J}_y} | JM' \rangle \equiv e^{-i\phi M} e^{-i\psi M'} d^J_{M,M'}(\theta). \tag{3.16}$$

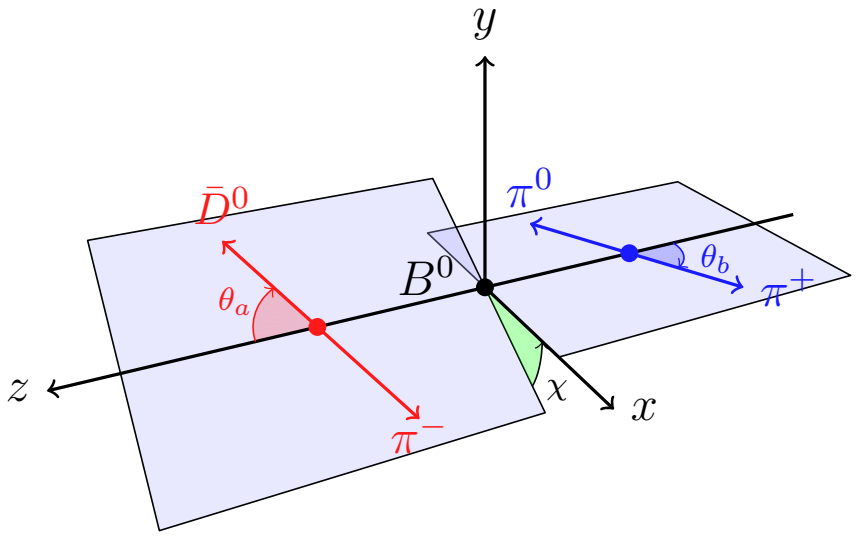

Figure 3.1: Helicity Basis

Now we are able to rewrite equation (3.13) as

$$A = \sum_{\lambda} H_\lambda \, e^{i\lambda\chi} \, d^{s_a *}_{\lambda,\lambda_{a_1}-\lambda_{a_2}}(\theta_a) \, d^{s_b *}_{\lambda,\lambda_{b_1}-\lambda_{b_2}}(\theta_b), \tag{3.17}$$

with

$$\chi = \phi_a + \phi_b. \tag{3.18}$$

Notice that the definition of the azimuthal angles ϕ_a, ϕ_b amounts to defining the phase convention of H_λ. In the following we will use the definition that the x axes are identical in both frames. That means χ is the azimuthal angle from b_1 to a_1 looking down from the a side. See Figure 3.1 for reference.

3.2 $B^0 \to D^{*-}\rho^+$ in Helicity Basis

We consider a decay of a neutral B^0 meson to charged D^{*-} and ρ^+ followed by

$$D^{*-} \to D^0\pi^-, \qquad \rho^+ \to \pi^+\pi^0. \tag{3.19}$$

Considering the particle labels of Section 3.1 we assign

$$\begin{aligned} D^{*-} &= a, \qquad D^0 = a_1, \qquad \pi^- = a_2, \\ \rho^+ &= b, \qquad \pi^+ = b_1, \qquad \pi^0 = b_2. \end{aligned} \tag{3.20}$$

As D^0 and $\pi^{\pm,0}$ have spin 0, their helicities also have to be 0, meaning that the decays of D^{*-} and ρ^+ have each but one helicity state. The general expression (3.17) then becomes

$$A = \sum_\lambda H_\lambda \, e^{i\lambda\chi} \, d^{1*}_{\lambda,0}(\theta_a) \, d^{1*}_{\lambda,0}(\theta_b) \tag{3.21}$$

In Wigner's sign convention [12] the d-functions are

$$d^{1*}_{1,0}(\theta) = -d^{1*}_{-1,0}(\theta) = -\frac{\sin\theta}{\sqrt{2}}, \qquad d^{1*}_{0,0}(\theta) = \cos\theta. \tag{3.22}$$

Combining the previous two equations yields

$$A = \sum_\lambda H_\lambda g_\lambda, \tag{3.23}$$

where for the sake of brevity we have introduced

$$\begin{aligned} g_{+1} &= \frac{1}{2} e^{i\chi} \sin\theta_a \sin\theta_b, \\ g_0 &= \cos\theta_a \cos\theta_b, \\ g_{-1} &= \frac{1}{2} e^{-i\chi} \sin\theta_a \sin\theta_b. \end{aligned} \tag{3.24}$$

The probability to obtain a certain result is thus proportional to

$$\begin{aligned} |A|^2 &= \left(\sum_\lambda H_\lambda g_\lambda \right) \left(\sum_\kappa H_\kappa g_\kappa \right)^* = \\ &= \sum_\lambda |H_\lambda|^2 |g_\lambda|^2 + 2\Re\left[H_{+1} g_{+1} (H^*_0 g^*_0 + H^*_{-1} g^*_{-1}) + H_0 g_0 \, H^*_{-1} g^*_{-1} \right] = \\ &= \sum_\lambda |H_\lambda|^2 |g_\lambda|^2 + 2 \sum_{\lambda<\kappa} \Re(H^*_\lambda g^*_\lambda \, H_\kappa g_\kappa). \end{aligned} \tag{3.25}$$

Notice that in the second term the Hs are 'entangled' with the gs under the $\Re$. As the gs can be directly evaluated while the Hs are parameters, it would be convenient if we could 'disentangle' them. This we can do because for general complex numbers a, b the following relation holds

$$\Re(ab) = \Re(a)\Re(b) - \Im(a)\Im(b). \tag{3.26}$$

Proving (3.26) is straightforward: we evaluate the left hand side and the right

hand side separately

$$\text{l.h.s.} = \frac{1}{2}(ab + a^* b^*) \tag{3.27}$$

$$\begin{aligned}\text{r.h.s.} &= \frac{1}{2}(a + a^*)\frac{1}{2}(b + b^*) - \frac{1}{2i}(a - a^*)\frac{1}{2i}(b - b^*) = \\ &= \frac{1}{4}[ab + \cancel{ab^*} + \cancel{a^* b} + a^* b^* + ab - \cancel{ab^*} - \cancel{a^* b} + a^* b^*] = \\ &= \frac{1}{2}(ab + a^* b^*) = \text{l.h.s.}\end{aligned} \tag{3.28}$$

If we take

$$a = H_\lambda^* H_\kappa, \qquad b = g_\lambda^* g_\kappa, \tag{3.29}$$

we can rewrite (3.25) as

$$|A|^2 = \sum_\lambda |H_\lambda|^2 |g_\lambda|^2 + 2\sum_{\lambda<\kappa} \left[\Re(H_\lambda^* H_\kappa)\Re(g_\lambda^* g_\kappa) - \Im(H_\lambda^* H_\kappa)\Im(g_\lambda^* g_\kappa)\right]. \tag{3.30}$$

To make the equations more readable we will now use the symbols $(+, 0, -)$ instead of $(+1, 0, -1)$ for labeling indices. To reach the final form of $|A|^2$ we will need these expressions, which we evaluate using standard trigonometric identities:

$$\Re(g_0^* g_+) = \frac{1}{2}\cos\theta_a \cos\theta_b \cos\chi \sin\theta_a \sin\theta_b = \frac{1}{8}\sin 2\theta_a \sin 2\theta_b \cos\chi \tag{3.31}$$

$$\Re(g_-^* g_+) = \frac{1}{4}\sin^2\theta_a \sin^2\theta_b \cos 2\chi \tag{3.32}$$

$$\Re(g_-^* g_0) = \Re(g_0^* g_+) \qquad \text{because } g_0^* = g_0 \text{ and } g_-^* = g_+ \tag{3.33}$$

$$\Im(g_0^* g_+) = \frac{1}{2}\cos\theta_a \cos\theta_b \sin\chi \sin\theta_a \sin\theta_b = \frac{1}{8}\sin 2\theta_a \sin 2\theta_b \sin\chi \tag{3.34}$$

$$\Im(g_-^* g_+) = \frac{1}{4}\sin^2\theta_a \sin^2\theta_b \sin 2\chi \tag{3.35}$$

$$\Im(g_-^* g_0) = \Im(g_0^* g_+) \qquad \text{because } g_0^* = g_0 \text{ and } g_-^* = g_+ \tag{3.36}$$

Putting it all together gives us the result

$$\begin{aligned}|A|^2 =&\frac{1}{4}(|H_+|^2+|H_-|^2)\sin^2\theta_a\sin^2\theta_b+|H_0|^2\cos^2\theta_a\cos^2\theta_b+\\&+\frac{1}{2}\left[\Re(H_-^*H_+)\cos 2\chi-\Im(H_-^*H_+)\sin 2\chi\right]\sin^2\theta_a\sin^2\theta_b+\\&+\frac{1}{4}\left\{\Re[(H_++H_-)H_0^*]\cos\chi-\Im[(H_+-H_-)H_0^*]\sin\chi\right\}\sin 2\theta_a\sin 2\theta_b.\end{aligned} \tag{3.37}$$

We now have the angular distribution up to a numerical normalization factor. For a normalized angular distribution Γ the integral over all angles is equal to unity. Therefore to find the normalization factor we integrate

$$I=\int_0^{2\pi}\mathrm{d}\chi\int_{-1}^{+1}\mathrm{d}\cos\theta_a\int_{-1}^{+1}\mathrm{d}\cos\theta_b\,|A|^2. \tag{3.38}$$

It is readily observable that the last two lines in equation (3.37) vanish when evaluating the integral over χ. Thus we are left with

$$I=2\pi\int_{-1}^{+1}\mathrm{d}\cos\theta_a\int_{-1}^{+1}\mathrm{d}\cos\theta_b\,\left[\frac{1}{4}(|H_+|^2+|H_-|^2)\sin^2\theta_a\sin^2\theta_b+|H_0|^2\cos^2\theta_a\cos^2\theta_b\right]. \tag{3.39}$$

Using

$$\int_{-1}^{+1}\mathrm{d}\cos\theta\,\sin^2\theta=\frac{4}{3},\qquad\int_{-1}^{+1}\mathrm{d}\cos\theta\,\cos^2\theta=\frac{2}{3}, \tag{3.40}$$

we arrive at the result

$$I=\frac{8\pi}{9}\left(|H_+|^2+|H_0|^2+|H_-|^2\right), \tag{3.41}$$

thus the normalized angular distribution is

$$\frac{\mathrm{d}^3\Gamma(\theta_a,\theta_b,\chi)}{\mathrm{d}\cos\theta_a\,\mathrm{d}\cos\theta_b\,\mathrm{d}\chi}=\frac{9}{8\pi}|A|^2, \tag{3.42}$$

if we use normalized helicity amplitudes, i.e., $\sum_\lambda|H_\lambda|^2=1$.

3.3 Transversity Basis

In many of the analyses conducted in B-factories, the final state is a CP eigenstate. In such a case it is often beneficial to use basis states that are CP eigenstates themselves. These define the so called transversity basis.

The final state in this analysis is not a CP eigenstate, nevertheless it will be useful to use the transversity basis as its basis states are P-eigenstates. To support that claim, let us look at the parity transformation of the two particle state (3.1) defined by [13]

$$\hat{P}|JM, \lambda_a\lambda_b\rangle = (-1)^{J-s_a-s_b}\pi_a\pi_b|JM, -\lambda_a-\lambda_b\rangle, \tag{3.43}$$

where s_a, s_b and π_a, π_b are the spins and intrinsic parities of the daughter particles, respectively. In our case [8]

$$J = M = 0, \qquad s_a = s_b = 1, \qquad \pi_a = \pi_b = -1, \tag{3.44}$$

implicating the states of (3.9) transform as

$$\hat{P}|f_+\rangle = |f_-\rangle, \qquad \hat{P}|f_0\rangle = |f_0\rangle, \qquad \hat{P}|f_-\rangle = |f_+\rangle \tag{3.45}$$

The longitudinal state $|f_0\rangle$ is P-even parity eigenstate, the other two states are an admixture of P-even and P-odd states. It is however easy to construct P-eigenstates from them. Writing

$$|f_\parallel\rangle = \frac{|f_+\rangle + |f_-\rangle}{\sqrt{2}} \qquad \text{P-even}, \tag{3.46}$$

$$|f_\perp\rangle = \frac{|f_+\rangle - |f_-\rangle}{\sqrt{2}} \qquad \text{P-odd}, \tag{3.47}$$

it is evident that these states are parity eigenstates.

To rewrite expression (3.8) in terms of the new transversity basis we define

new *transversity* amplitudes

$$\begin{aligned} A_{\parallel} &= \frac{H_+ + H_-}{\sqrt{2}}, \\ A_0 &= H_0, \\ A_{\perp} &= \frac{H_+ - H_-}{\sqrt{2}}. \end{aligned} \tag{3.48}$$

Rewriting (3.8) is now trivial

$$|\psi_f\rangle = \sum_m A_m |f_m\rangle, \qquad m \in \{\parallel, 0, \perp\}. \tag{3.49}$$

Now we need to define some angle convention for the transversity basis. We start by taking the helicity basis convention depicted in Figure 3.1. Notice the x-axis is taken to be in the decay plane of the particle we designated as b in (3.20) and in such a way that b_1 travels in the positive direction. We now define a new coordinate system by transforming

$$x \to y', \qquad y \to z', \qquad z \to x' \tag{3.50}$$

and we introduce two new angles (θ_t, ϕ_t) that are the polar coordinates of particle a_1 in the new basis. This gives us an often used [14] set of angles $(\theta_t, \theta_b, \phi_t)$ for the transversity basis. It is simple to find the relation between the original set of angles and the new one

$$\begin{aligned} x &= \sin\theta_a \cos\chi &&= \sin\theta_t \sin\phi_t &&= y' \\ y &= \sin\theta_a \sin\chi &&= \cos\theta_t &&= z' \\ z &= \cos\theta_a &&= \sin\theta_t \cos\phi_t &&= y' \end{aligned} \tag{3.51}$$

We can use equations (3.51) to express the angular distribution in terms of the transversity angles. In analogy to equation (3.23) we can write

$$A = \sum_m A_m g_m \tag{3.52}$$

and g_m have to be defined consistently with A_m (see (3.48)), i.e.,

$$\begin{aligned} g_{\parallel} &= \frac{g_+ + g_-}{\sqrt{2}} = \frac{1}{\sqrt{2}} \sin\theta_a \sin\theta_b \cos\chi = \frac{1}{\sqrt{2}} \sin\theta_t \sin\theta_b \sin\phi_t \\ g_0 &= g_0 \qquad\quad = \cos\theta_a \cos\theta_b \qquad\quad = \sin\theta_t \cos\theta_b \cos\phi_t \\ g_{\perp} &= \frac{g_+ - g_-}{\sqrt{2}} = \frac{i}{\sqrt{2}} \sin\theta_a \sin\theta_b \sin\chi = \frac{i}{\sqrt{2}} \cos\theta_t \sin\theta_b \end{aligned} \tag{3.53}$$

where we have used the exponential sine and cosine form

$$\sin\chi = \frac{1}{2i}(e^{i\chi} - e^{-i\chi}), \qquad \cos\chi = \frac{1}{2}(e^{i\chi} + e^{-i\chi}) \tag{3.54}$$

for the first column of equations and relations (3.51) for the second column.

It is noteworthy that we could use relations (3.51) directly, i.e., we didn't need to express, e.g., $\sin\theta_a$ by itself. We needed only those combinations present in (3.51). This is not a coincidence but a consequence of the so called 'addition theorem for spherical harmonics' [15] which is a trigonometric identity generalized to more dimensions.

Similarly to (3.25) we will have to compute $|A|^2$, this time by squaring (3.52). If we define a formal ordering for the indices m, e.g., $(\parallel > 0 > \perp)$ we can directly reuse (3.30) writing

$$|A|^2 = \sum_m |A_m|^2 |g_m|^2 + 2 \sum_{m<n} \big[\Re(A_m A_n^*) \Re(g_m g_n^*) - \Im(A_m A_n^*) \Im(g_m g_n^*) \big]. \tag{3.55}$$

Notice both $g_{\parallel}$ and g_0 are real, while $g_{\perp}$ is purely imaginary. Thus their products are also either real or purely imaginary. This fact allows us to simplify (3.55) because either the first or the second term in the second sum is 0. Consequently we can transcribe the last equation as

$$|A|^2 = \sum_m |A_m|^2 |g_m|^2 + 2 \big[\Re(A_0 A_{\parallel}^*) \Re(g_0 g_{\parallel}^*) - \Im(A_{\perp} A_{\parallel}^*) \Im(g_{\perp} g_{\parallel}^*) - \Im(A_{\perp} A_0^*) \Im(g_{\perp} g_0^*) \big]. \tag{3.56}$$

As in Section 3.2, we find the explicit forms:

$$\Re(g_0 g_\parallel^*) = \frac{1}{\sqrt{2}} \sin^2\theta_t \sin\theta_b \cos\theta_b \sin\phi_t \cos\phi_t = \frac{1}{4\sqrt{2}} \sin^2\theta_t \sin 2\theta_b \sin 2\phi_t \quad (3.57)$$

$$\Im(g_\perp g_\parallel^*) = \frac{1}{2} \sin\theta_t \cos\theta_t \sin^2\theta_b \sin\phi_t = \frac{1}{4} \sin 2\theta_t \sin^2\theta_b \sin\phi_t \quad (3.58)$$

$$\Im(g_\perp g_0^*) = \frac{1}{\sqrt{2}} \sin\theta_t \cos\theta_t \sin\theta_b \cos\theta_b \cos\phi_t = \frac{1}{4\sqrt{2}} \sin 2\theta_t \sin 2\theta_b \cos\phi_t \quad (3.59)$$

Combining the above equations and taking into account the normalization factor from (3.42) (the transformations we employed were actually unitary, i.e., respecting the inner product and thus normalization), we arrive at the expression for angular distribution in terms of the transversity angles

$$\begin{aligned}\frac{\mathrm{d}^3\Gamma(\theta_t,\theta_b,\phi_t)}{\mathrm{d}\cos\theta_t\,\mathrm{d}\cos\theta_b\,\mathrm{d}\phi_t} = \frac{9}{32\pi}\Big\{ & 2|A_\parallel|^2 \sin^2\theta_t \sin^2\theta_b \sin^2\phi_t + 2|A_\perp|^2 \cos^2\theta_t \sin^2\theta_b + \\ & + 4|A_0|^2 \sin^2\theta_t \cos^2\theta_b \cos^2\phi_t + \sqrt{2}\Re(A_0 A_\parallel^*) \sin^2\theta_t \sin 2\theta_b \sin 2\phi_t - \\ & - 2\Im(A_\perp A_\parallel^*) \sin 2\theta_t \sin^2\theta_b \sin\phi_t - \sqrt{2}\Im(A_\perp A_0^*) \sin 2\theta_t \sin 2\theta_b \cos\phi_t \Big\},\end{aligned} \quad (3.60)$$

which is identical to the distribution given in [14].

3.4 Time-Dependent Analysis

In this Section we will investigate the time dependence of the angular distribution.

Let us begin by looking at the time evolution of the B meson states. This evolution is of course described by the time-dependent Schrödinger equation

$$i\frac{\partial}{\partial t}\Psi = \hat{H}\Psi, \qquad \Psi = \begin{pmatrix} |B^0\rangle \\ |\bar{B}^0\rangle \end{pmatrix}. \quad (3.61)$$

The effective Hamiltonian that leads to a decay can be described by

$$\hat{H}_{\text{eff}} = \hat{M} - i\frac{\hat{\Gamma}}{2} = \left[\begin{pmatrix} M_{11} & M_{12} \\ M_{21} & M_{22} \end{pmatrix} - \frac{i}{2} \begin{pmatrix} \Gamma_{11} & \Gamma_{12} \\ \Gamma_{21} & \Gamma_{22} \end{pmatrix} \right], \quad (3.62)$$

where the operator $\hat{M}$ is the probability conserving, hermitian part, while $-i\frac{\hat{\Gamma}}{2}$ is the non-hermitian part responsible for particle decay. The CPT symmetry implies

$$M_{11} = M_{22} \equiv m, \qquad M_{12} = M_{21}^* \equiv \mu, \tag{3.63}$$

$$\Gamma_{11} = \Gamma_{22} \equiv \gamma, \qquad \Gamma_{12} = \Gamma_{21}^*. \tag{3.64}$$

Moreover there is no or negligible direct decay CP violation in the B_d system (B mesons containing a d quark/antiquark) we study, i.e., $\Gamma_{12} = \Gamma_{21} \doteq 0$ [16]. This means the decay part of the Hamiltonian will result only in a factor of $e^{-\frac{\gamma}{2}t}$ when evolving both B states. We will drop this factor for now and restore it later.

Solving the evolution equation (3.61) amounts to finding eigenvectors and the corresponding eigenvalues of the evolution operator. Setting

$$\det\left[\begin{pmatrix} m & \mu \\ \mu^* & m \end{pmatrix} - \lambda \begin{pmatrix} 1 & 0 \\ 0 & 1 \end{pmatrix}\right] = 0 \tag{3.65}$$

leads to the characteristic equation

$$(m-\lambda)^2 - |\mu|^2 = 0 \tag{3.66}$$

with the obvious solutions

$$\lambda_{1,2} = m \pm |\mu|. \tag{3.67}$$

We define the heavier state as an arbitrary linear combination of both B meson states with definite quark content (flavor), e.g., as

$$|B_H\rangle = p_H|B^0\rangle + q_H|\bar{B}^0\rangle, \tag{3.68}$$

with p_H, q_H being complex numbers satisfying

$$|p_H|^2 + |q_H|^2 = 1 \tag{3.69}$$

to keep the normalization. For the heavier eigenstate the following has to hold

$$\begin{pmatrix} m & \mu \\ \mu^* & m \end{pmatrix} \begin{pmatrix} p_H \\ q_H \end{pmatrix} = (m + |\mu|) \begin{pmatrix} p_H \\ q_H \end{pmatrix} \tag{3.70}$$

or equivalently

$$\begin{aligned} m\, p_H + \mu\, q_H = (m + |\mu|) p_H \quad &\Longrightarrow \quad \frac{p_H}{q_H} = \frac{\mu}{|\mu|}, \\ \mu^* p_H + m\, q_H = (m + |\mu|) q_H \quad &\Longrightarrow \quad \frac{q_H}{p_H} = \frac{\mu^*}{|\mu|}, \end{aligned} \tag{3.71}$$

thus we get an interesting relation

$$\left(\frac{p_H}{q_H}\right)^* = \frac{q_H}{p_H}. \tag{3.72}$$

The same process done with the lighter state yields

$$\begin{aligned} \frac{p_L}{q_L} &= -\frac{\mu}{|\mu|}, \\ \frac{q_L}{p_L} &= -\frac{\mu^*}{|\mu|}, \end{aligned} \tag{3.73}$$

meaning we can take, e.g.,

$$p_H = p_L \equiv p, \qquad q_H = -q_L \equiv q. \tag{3.74}$$

Subsequently the two eigenstates can be written as

$$|B_H\rangle = p|B^0\rangle + q|\bar{B}^0\rangle, \qquad |B_L\rangle = p|B^0\rangle - q|\bar{B}^0\rangle \tag{3.75}$$

and their evolution is simply

$$|B_H(t)\rangle = e^{-im_H t}|B_H\rangle, \qquad |B_L(t)\rangle = e^{-im_L t}|B_L\rangle, \tag{3.76}$$

where we have introduced $m_{H,L} = m \pm |\mu|$.

The total phase is irrelevant as long as we keep the relative phase between $|B_H(t)\rangle$ and $|B_L(t)\rangle$ intact. Thus we may multiply both terms from (3.76) by

$e^{i(m_H+m_L)/2}$, resulting in the convenient expressions

$$|B_H(t)\rangle = e^{-i\Delta m_d\, t}|B_H\rangle, \qquad |B_L(t)\rangle = e^{i\Delta m_d\, t}|B_L\rangle, \tag{3.77}$$

where we have introduced $\Delta m_d = m_H - m_L$.

To get the time evolution of the flavor eigenstates $B^0, \bar{B}^0$ we have to solve the equation system (3.75) with respect to them:

$$|B^0\rangle = \frac{|B_H\rangle + |B_L\rangle}{2p}, \qquad |\bar{B}^0\rangle = \frac{|B_H\rangle - |B_L\rangle}{2q} \tag{3.78}$$

Combining (3.75), (3.77),(3.78) and restoring the factor $e^{-\frac{\gamma}{2}t}$ yields the complete time evolution of pure $B^0, \bar{B}^0$ states

$$\begin{aligned} |B^0(t)\rangle &= e^{-\frac{\gamma}{2}t}\left(|B^0\rangle \cos\frac{\Delta m_d\, t}{2} - \frac{q}{p}|\bar{B}^0\rangle i \sin\frac{\Delta m_d\, t}{2}\right), \\ |\bar{B}^0(t)\rangle &= e^{-\frac{\gamma}{2}t}\left(|\bar{B}^0\rangle \cos\frac{\Delta m_d\, t}{2} - \frac{p}{q}|B^0\rangle i \sin\frac{\Delta m_d\, t}{2}\right). \end{aligned} \tag{3.79}$$

Before we atempt to use these formulas, we need to now when was $t = 0$, i.e. when the B mesons were in a definite flavor state. This is where the B-factory B meson production scheme comes in. The B mesons come from a decay of an $\Upsilon(4S)$ particle, which is a boson, thus it has a symmetric wavefunction. As the spin of the system has to be conserved and the resulting mesons are scalars, they have to be in a state with a net angular momentum of 1. The spherical harmonic functions associated with an angular momentum of 1 are anti-symmetric [17], i.e., the spatial part of the wave function of the B pair is anti-symmetric. This can be counteracted only by the flavor part of the wave function, which has to be anti-symmetric as well, so that their product is symmetric. This means that up to a numeric factor the flavor part of the wave function is

$$|B^0\bar{B}^0\rangle = |B^0\rangle|\bar{B}^0\rangle - |\bar{B}^0\rangle|B^0\rangle. \tag{3.80}$$

We can see that the states $|B^0\rangle$ and $|\bar{B}^0\rangle$ are *entangled*. Thus in the moment one of the B mesons decays, if we can tag its flavor, we know that the other one is in that instant in the oposite pure flavor state, which means we have our $t = 0$.

Let us digress a bit now and consider the reason why there should be a (potentially) observable CP violation present in the studied channel. There are three types of CP violation present in the Standard Model [16]:

- **CP violation in decays**, which is caused by different rates for a process with respect to its CP conjugate. (Not measurable in the studied channel.)
- **Indirect CP violation** , which emerges from mixing when $|p/q| \neq 1$. (Not true in our approximation as attested by (3.71).)
- **Mixing induced CP violation**, when there is interference between $B \to f$ and $B \to \bar{B} \to f$.

The only possible CP violation we are left with is the mixing induced one. For it to take place, both B and $\bar{B}$ must be able to decay to the same final state. To convince ourselves that this is indeed possible in the studied channel, take a look at the Feynman diagrams in Figure 3.2. All the depicted decays are of a B^0 meson but the final state in the upper two diagrams is $D^{*-}\rho^+$ while in the lower pair it is the charge conjugated state $D^{*+}\rho^-$. To get an idea about the magnitude of the corresponding amplitudes, one can inspect the charged current Lagrangian [18]:

$$\mathcal{L}_{\mathrm{CC}} = \frac{g}{2\sqrt{2}}\big(\bar{u}\ \bar{c}\ \bar{t}\big)\gamma^{\mu}(1-\gamma_5)\begin{pmatrix} V_{ud} & V_{us} & V_{ub} \\ V_{cd} & V_{cs} & V_{cb} \\ V_{td} & V_{ts} & V_{tb} \end{pmatrix}\begin{pmatrix} d \\ s \\ l \end{pmatrix} W_{\mu}^{+} + \mathrm{h.c.} \tag{3.81}$$

where the 'V matrix' is the Cabibbo-Kobayashi-Maskawa (CKM) quark mixing matrix. We see that the amplitudes of the upper pair of diagrams from Figure 3.2 are proportional to $V_{cb}^{*}V_{ud}$ while the lower pair to $V_{ub}^{*}V_{cd}$. The magnitudes of these CKM matrix elements are [8]

$$\begin{aligned} |V_{ud}| &\approx 0.974, \quad |V_{cb}| \approx 0.041 \\ |V_{cd}| &\approx 0.225, \quad |V_{ub}| \approx 0.003 \end{aligned} \tag{3.82}$$

These hint that the amplitudes of the former pair of diagrams will be very roughly 60 times larger than the latter because of the CKM matrix elements' magnitudes.

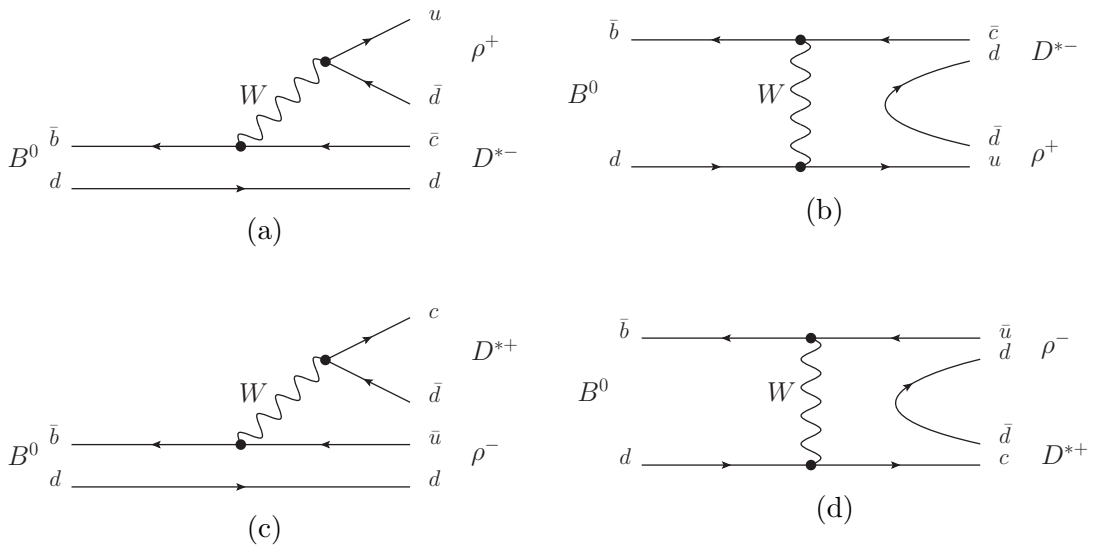

Figure 3.2: Feynman diagrams of $B_0 \to D^*\rho$ decays

Because of this the upper type is called *Cabibbo favored* and the lower *(Doubly) Cabibbo suppressed* decay.

We can check that this estimate is not completely wrong by looking at the measured branching fractions of $B^0 \to D^{\mp}\rho^{\pm}$. The ratio of these branching fractions is ≈ 3436 [8], while our guess would be $60^2 = 3600$, which is remarkably close. Take note, that there is no guarantee that the ratio will be as close to this estimate for the studied channel and so we will use it only as a hint to the order of magnitude of the ratio.

It is rather apparent that we can charge conjugate all the diagrams in Figure 3.2 to get the corresponding diagrams for a $\bar{B}^0$ meson for which the favored and suppressed final states are switched.

We now define twelve instantaneous decay amplitudes:

$$\begin{aligned} a_m &\equiv A_{B^0\to f_m} = V_{cb}^* V_{ud} F_{cm} \\ \bar{a}_m &\equiv A_{\bar{B}^0\to \bar{f}_m} = V_{cb} V_{ud}^* \bar{F}_{cm} \\ b_m &\equiv A_{B^0\to \bar{f}_m} = V_{ub}^* V_{cd} F_{um} \qquad m \in \{\|, 0, \perp\}, \\ \bar{b}_m &\equiv A_{\bar{B}^0\to f_m} = V_{ub} V_{cd}^* \bar{F}_{um} \end{aligned} \tag{3.83}$$

where we have introduced $f \equiv D^{*-}\rho^+$ and $\bar{f} \equiv D^{*+}\rho^-$ for the sake of brevity and in the second column we have separated the CKM factors from the amplitude, designating the rest as F_{qm}.

We now write down the time-dependent amplitudes for a definite flavor B state decaying to the six possible final states:

$$A_{B^0\to f_m}(t) = e^{-\frac{\gamma}{2}t}\left(a_m \cos\frac{\Delta m_d\, t}{2} - \frac{q}{p}\bar{b}_m i \sin\frac{\Delta m_d\, t}{2}\right) \tag{3.84}$$

$$A_{\bar{B}^0\to \bar{f}_m}(t) = e^{-\frac{\gamma}{2}t}\left(\bar{a}_m \cos\frac{\Delta m_d\, t}{2} - \frac{p}{q} b_m i \sin\frac{\Delta m_d\, t}{2}\right) \tag{3.85}$$

$$A_{B^0\to \bar{f}_m}(t) = e^{-\frac{\gamma}{2}t}\left(b_m \cos\frac{\Delta m_d\, t}{2} - \frac{q}{p}\bar{a}_m i \sin\frac{\Delta m_d\, t}{2}\right) \tag{3.86}$$

$$A_{\bar{B}^0\to f_m}(t) = e^{-\frac{\gamma}{2}t}\left(\bar{b}_m \cos\frac{\Delta m_d\, t}{2} - \frac{p}{q} a_m i \sin\frac{\Delta m_d\, t}{2}\right) \tag{3.87}$$

We can simplify these equations by introducing

$$\rho_m = \frac{q\,\bar{b}_m}{p\,a_m}, \qquad \bar{\rho}_m = \frac{p\,b_m}{q\,\bar{a}_m} \tag{3.88}$$

and ignoring the overall phase factor $\frac{q}{p}$ and $\frac{p}{q}$ in equations (3.86), (3.87), respectively. Equation (3.71) attests they are just phase factors, i.e., $\left|\frac{q}{p}\right| = \left|\frac{p}{q}\right| = 1$. Thus we arrive at

$$A_{B^0\to f_m}(t) = e^{-\frac{\gamma}{2}t} a_m \left(\cos\frac{\Delta m_d\, t}{2} - \rho_m i \sin\frac{\Delta m_d\, t}{2}\right) \tag{3.89}$$

$$A_{\bar{B}^0\to \bar{f}_m}(t) = e^{-\frac{\gamma}{2}t} \bar{a}_m \left(\cos\frac{\Delta m_d\, t}{2} - \bar{\rho}_m i \sin\frac{\Delta m_d\, t}{2}\right) \tag{3.90}$$

$$A_{B^0\to \bar{f}_m}(t) = e^{-\frac{\gamma}{2}t} \bar{a}_m \left(\bar{\rho}_m \cos\frac{\Delta m_d\, t}{2} - i \sin\frac{\Delta m_d\, t}{2}\right) \tag{3.91}$$

$$A_{\bar{B}^0\to f_m}(t) = e^{-\frac{\gamma}{2}t} a_m \left(\rho_m \cos\frac{\Delta m_d\, t}{2} - i \sin\frac{\Delta m_d\, t}{2}\right) \tag{3.92}$$

We now examine the parameters ρ_m as they are crucial in this analysis. Combining (3.83) with the definition (3.88) leads to

$$\rho_m = \frac{q}{p}\frac{V_{ub}V_{cd}^*}{V_{cb}^*V_{ud}}\frac{\bar{F}_{um}}{F_{cm}} \tag{3.93}$$

According to [14], assuming CP is violated solely through the weak phases,

the following relations hold

$$F_{q\parallel} = \bar{F}_{q\parallel}, \qquad F_0 = \bar{F}_0, \qquad F_{q\perp} = -\bar{F}_{q\perp} \tag{3.94}$$

and

$$\frac{q}{p} = -\frac{V_{td}V_{tb}^*}{V_{td}^*V_{tb}}. \tag{3.95}$$

We can now rewrite (3.88) as

$$\begin{aligned} \rho_m &= \frac{q\,\bar{b}_m}{p\,a_m} = \frac{q\,V_{ub}V_{cd}^*\bar{F}_{um}}{p\,V_{cb}^*V_{ud}F_{cm}} = -\frac{V_{td}V_{tb}^*V_{ub}V_{cd}^*\bar{F}_{um}}{V_{td}^*V_{tb}V_{cb}^*V_{ud}F_{cm}} \equiv r_m e^{i\phi_{\rho m}} \\ \bar{\rho}_m &= \frac{p\,b_m}{q\,\bar{a}_m} = \frac{p\,V_{ub}^*V_{cd}F_{um}}{q\,V_{cb}V_{ud}^*\bar{F}_{cm}} = -\frac{V_{td}^*V_{tb}V_{ub}^*V_{cd}F_{um}}{V_{td}V_{tb}^*V_{cb}V_{ud}^*\bar{F}_{cm}} \equiv r_m e^{i\phi_{\bar{\rho}m}} \end{aligned} \tag{3.96}$$

We continue by introducing the so called unitarity triangles and their internal angles which can be used to simplify expressions (3.96). The CKM matrix is unitary [19] and thus subject to certain constaints. Namely elements of a unitary matrix V satisfy

$$(V^\dagger V)_{ij} = (VV^\dagger)_{ij} = \delta_{ij}. \tag{3.97}$$

For a 3x3 unitary matrix such as the CKM matrix, this translates into nine conditions. The six relations with $i \neq j$ define a triangle in the complex plane, as a sum of any three complex numbers equal to zero does (although the triangle can be degenerate). By convention the triangle defined by

$$V_{ud}V_{ub}^* + V_{cd}V_{cb}^* + V_{td}V_{tb}^* = 0 \tag{3.98}$$

is used for defining unitarity angles. This choice has the benefit of the angles being of equal order, hence they can be measured independently with reasonable relative errors.

We define the unitarity angles according to Figure 3.3. Writing them out

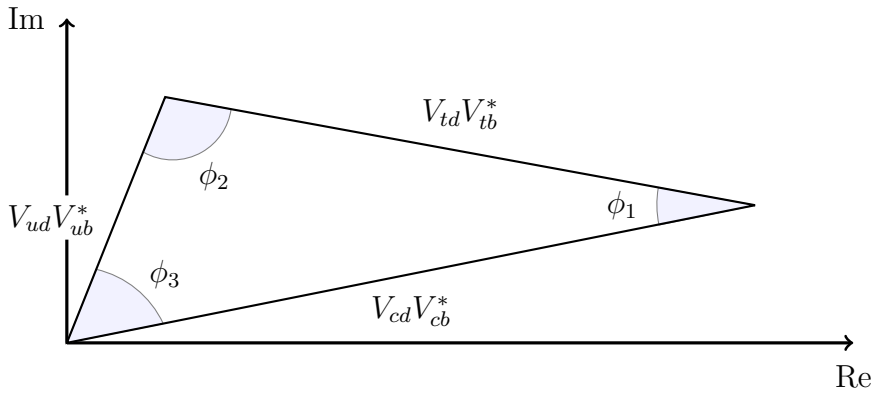

Figure 3.3: Unitarity triangle in the complex plane

explicitly yields

$$\begin{aligned}\phi_1 &= \arg\left(-\frac{V_{cd}V_{cb}^*}{V_{td}V_{tb}^*}\right),\\ \phi_2 &= \arg\left(-\frac{V_{td}V_{tb}^*}{V_{ud}V_{ub}^*}\right),\\ \phi_3 &= \arg\left(-\frac{V_{ud}V_{ub}^*}{V_{cd}V_{cb}^*}\right).\end{aligned} \tag{3.99}$$

Using these angle definitions we can make out the phases of ρ_m and $\bar{\rho}_m$. Taking, e.g., the latter we get

$$\begin{aligned}\arg\bar{\rho}_m &= \arg\left(-\frac{V_{td}^*V_{tb}V_{ub}^*V_{cd}}{V_{td}V_{tb}^*V_{cb}V_{ud}^*}\right) + \arg\left(\frac{F_{um}}{\bar{F}_{cm}}\right) =\\ &= \arg\left(-\frac{V_{cd}V_{cb}^*}{V_{td}V_{tb}^*}\frac{V_{cd}V_{cb}^*}{V_{td}V_{tb}^*}\frac{V_{ud}V_{ub}^*}{V_{cd}V_{cb}^*}\right) + \arg\left(\frac{F_{um}}{\bar{F}_{cm}}\right) =\\ &= 2\phi_1 + \phi_3 + \delta_m,\end{aligned} \tag{3.100}$$

where we have introduced

$$\delta_m \equiv \arg\frac{F_{um}}{\bar{F}_{cm}}, \tag{3.101}$$

the so called *strong phase*. Taking into account relations (3.94) we see that also

$$\frac{F_{um}}{\bar{F}_{cm}} = \frac{\bar{F}_{um}}{F_{cm}} \tag{3.102}$$

and thus we have

$$\begin{aligned}\arg\rho_m &= \arg\left[\left(-\frac{V_{td}^*V_{tb}V_{ub}^*V_{cd}}{V_{td}V_{tb}^*V_{cb}V_{ud}^*}\right)^*\right] + \arg\left(\frac{\bar{F}_{um}}{F_{cm}}\right) = \\ &= -\arg\left(-\frac{V_{td}^*V_{tb}V_{ub}^*V_{cd}}{V_{td}V_{tb}^*V_{cb}V_{ud}^*}\right) + \delta_m = \\ &= -2\phi_1 - \phi_3 + \delta_m,\end{aligned} \tag{3.103}$$

where we have used the fact that for a general complex number z

$$\arg z^* = -\arg z. \tag{3.104}$$

Now we can rewrite (3.96) into the final form

$$\begin{aligned}\rho_m &= r_m e^{i(-\phi_w+\delta_m)}, \\ \bar{\rho}_m &= r_m e^{i(+\phi_w+\delta_m)},\end{aligned} \tag{3.105}$$

where we have introduced $\phi_w \equiv 2\phi_1 + \phi_3$.

We would like to stress that different strong phase definitions are sometimes introduced, such as the one in [14] where the authors use

$$\delta'_m \equiv \arg\frac{F_{um}}{F_{cm}} \tag{3.106}$$

The relation to our δ_m is (taking into account (3.94)):

$$\delta_\parallel = \delta'_\parallel, \qquad \delta_0 = \delta'_0, \qquad \delta_\perp = \delta'_\perp + \pi. \tag{3.107}$$

To get the final time-dependent angular distribution we only have to change $A_m \to A_m(t)$ in (3.60). Of course we have four final angular distributions since we have four decay modes as seen in equations (3.89) - (3.92).

Let us start with the $B^0 \to f$, i.e., $B^0 \to D^{*-}\rho^+$ mode. We need to evaluate the following terms, which is straightforward, but rather tedious. After exploiting (3.105), applying standard trigonometric identities and reordering the result, we

obtain

$$|A_{B^0\to f_m}|^2 = |a_m|^2\big[(1+r_m^2)+(1-r_m^2)\cos\delta mt - r_m\sin\delta mt\sin(\phi_w-\delta_m)\big] \quad (3.108)$$

$$\begin{aligned}
&\Re\big(A_{B^0\to f_0}(t)A^*_{B^0\to f_\parallel}(t)\big) = \\
&= +\,\Re(a_0a_\parallel^*)(1+r_0r_\parallel\cos(\delta_0-\delta_\parallel)) - \Im(a_0a_\parallel^*)r_0r_\parallel\sin(\delta_0-\delta_\parallel)+ \\
&\quad +\big[\Re(a_0a_\parallel^*)(1-r_0r_\parallel\cos(\delta_0-\delta_\parallel)) + \Im(a_0a_\parallel^*)r_0r_\parallel\sin(\delta_0-\delta_\parallel)\big]\cos\Delta m_d\,t- \\
&\quad -\big[\Re(a_0a_\parallel^*)(r_0\sin(\phi_w-\delta_0)+r_\parallel\sin(\phi_w-\delta_\parallel))- \\
&\quad -\Im(a_0a_\parallel^*)(r_0\cos(\phi_w-\delta_0)-r_\parallel\cos(\phi_w-\delta_\parallel))\big]\sin\Delta m_d\,t
\end{aligned} \quad (3.109)$$

$$\begin{aligned}
&\Im\big(A_{B^0\to f_\perp}(t)A^*_{B^0\to f_e}(t)\big) = \\
&= +\,\Im(a_\perp a_e^*)(1-r_\perp r_e\cos(\delta_\perp-\delta_e)) - \Re(a_\perp a_e^*)r_\perp r_e\sin(\delta_\perp-\delta_e)+ \\
&\quad +\big[\Im(a_\perp a_e^*)(1+r_\perp r_e\cos(\delta_\perp-\delta_e)) + \Re(a_\perp a_e^*)r_\perp r_e\sin(\delta_\perp-\delta_e)\big]\cos\Delta m_d\,t+ \\
&\quad +\big[\Im(a_\perp a_e^*)(r_\perp\sin(\phi_w-\delta_\perp)-r_e\sin(\phi_w-\delta_e))+ \\
&\quad +\Re(a_\perp a_e^*)(r_\perp\cos(\phi_w-\delta_\perp)+r_e\cos(\phi_w-\delta_e))\big]\sin\Delta m_d\,t
\end{aligned} \quad (3.110)$$

where we have introduced the index $e \in \{\parallel, 0\}$. Getting the final time-dependent angular distribution function for the chosen mode is as easy as exchanging expressions (3.108) - (3.110) for their time-independent analogues in the distribution (3.60).

One could carry out similar calculations to get these expressions for the other three modes, but there is a more elegant way. Returning to equations (3.89) - (3.92) we can notice that by changing $\Delta m_d\,t \to \Delta m_d\,t + \pi$ we get

$$\begin{aligned}
A_{B^0\to f_m}(t) &\to e^{-\frac{\gamma}{2}t}a_m\left[\cos\left(\frac{\Delta m_d\,t}{2}+\frac{\pi}{2}\right) - \rho_m i\sin\left(\frac{\Delta m_d\,t}{2}+\frac{\pi}{2}\right)\right] = \\
&= e^{-\frac{\gamma}{2}t}a_m\left[-\sin\left(\frac{\Delta m_d\,t}{2}\right) - \rho_m i\cos\left(\frac{\Delta m_d\,t}{2}\right)\right] = \\
&= (-i)e^{-\frac{\gamma}{2}t}a_m\left[\rho_m\cos\left(\frac{\Delta m_d\,t}{2}\right) - i\sin\left(\frac{\Delta m_d\,t}{2}\right)\right] = \\
&= (-i)A_{\bar{B}^0\to f_m}(t)
\end{aligned} \quad (3.111)$$

and similarly

$$A_{\bar{B}^0\to \bar{f}_m}(t) \to (-i)A_{B^0\to \bar{f}_m}(t) \quad (3.112)$$

The extra $(-i)$ is not a nuisance as it is only a global phase factor, which does not manifest in any physical observables. So for our intents and purposes we can say that changing $\Delta m_d\, t \to \Delta m_d\, t + \pi$ changes a B^0 decay to a certain final state to a $\bar{B}^0$ decay to the same final state and vice versa.

Moreover exchanging $\phi_w \leftrightarrow -\phi_w$ transforms $\rho_m \leftrightarrow \bar{\rho}_m$ as is readily observable in (3.105), thus transforming

$$\begin{aligned} A_{B^0 \to f_m}(t) &\leftrightarrow A_{B^0 \to \bar{f}_m}(t) \\ A_{\bar{B}^0 \to f_m}(t) &\leftrightarrow A_{\bar{B}^0 \to \bar{f}_m}(t) \end{aligned} \tag{3.113}$$

again up to a total, irrelevant, phase factor.

Using these simple transformations in (3.108) - (3.110) we can easily reach the angular distributions for any of the four modes from the one mode we actually calculated.

It is noteworthy that we could employ the remarkably simple transformation (3.113) because of the transversity basis. Had we used helicity basis, it would not have been quite so simple.

Chapter 4

Software

4.1 Implementation

The analysis' software implementation can be divided into three levels, as illustrated in Figure 4.1. First we will give a general description of the individual steps and later in this Chapter we will review each on in more detail.

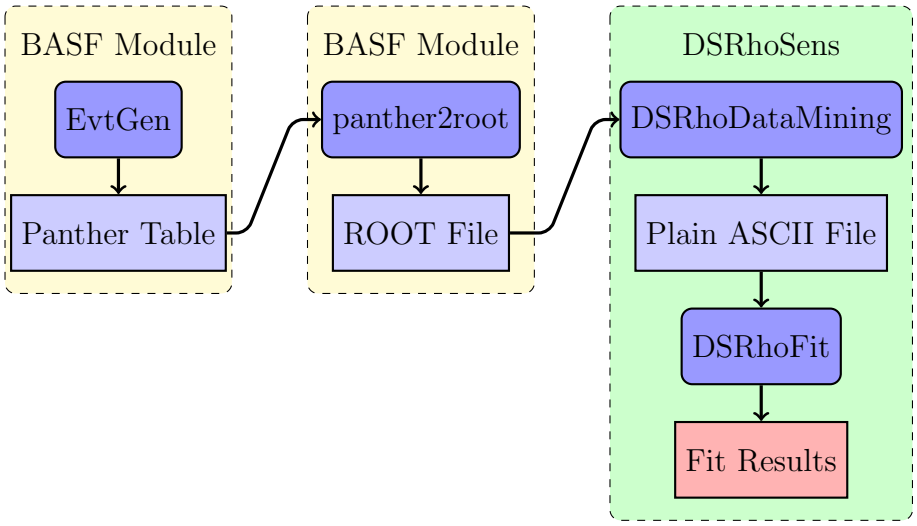

Figure 4.1: Workflow

We begin by generating events using the EvtGen Monte Carlo generator [20]. This is a well established event generator specifically designed for the simulation of physics of B decays and is widely used in both Belle and BaBar collaborations. One of the main focuses of this study is to verify this generator for scalar $\rightarrow$ vector + vector decays, where the final state is not a CP eigenstate. In

other words to verify a specific EvtGen model called '`SVV_NONCPEIGEN`'.

We do this in two steps: first, we will validate a model called '`SVV_HELAMP`' that is used to decay an arbitrary scalar particle to two vector ones, without any CP violation. The helicity amplitudes are supplied as arguments to the model. This model is important, because the model of real interest to us, `SVV_NONCPEIGEN`, computes the time-dependent effects like mixing and CP violation and then hands the rest of the work to `SVV_HELAMP`. The second step is a direct verification of our time-dependent fitter and `SVV_NONCPEIGEN` by means of the time-dependent analysis.

The EvtGen generator is integrated in the BASF framework used in the Belle experiment [21]. It is a modular system that uses various libraries written in Fortran, C and C++. User programs are actually modules for the framework.

After we have generated the data, BASF saves them as a PANTHER table. This is not very convenient as the main body of the analysis software uses just the ROOT framework [22]. Thus the next step is to convert the PANTHER table into a ROOT tree. This is facilitated by a short program I wrote, called '`panther2root`'. Again, it is actually a BASF module.

Once we have all the data in a ROOT friendly format we can start extracting the relevant observables. These in our case are the three transversity/helicity angles, the time difference between the decay of B^0 and $\bar{B}^0$ mesons and the decay type (see equations (3.89) - (3.92)). The extraction or 'data mining' is handled by a program we called '`DSRhoDataMining`'.

The last step is retrieving the physical parameters of the model, which are:

- 3 complex instantaneous amplitudes of transversity/helicity states

  $A_m = \langle f_m | H_{\text{eff}} | B_0 \rangle$

- 3 real *strong phases* δ_m

- 3 real coefficients r_m (the ratio $|A_{B^0 \to \bar{f}_m} / A_{B^0 \to f_m}|$)

- 1 real *weak phase* $\phi_w = 2\phi_1 + \phi_3$

Generally, having three complex parameters is equivalent to having six real ones, but taking into account that we want the instantaneous amplitudes normalized,

we have a constraint condition $\sum_m |A_m|^2 = 1$. Moreover only the relative phases between them are physical, meaning we can fix the phase of, e.g., A_0 setting it to 0, thus losing another degree of freedom.

There are $(6-2)+3+3+1 = 11$ parameters altogether.

It is worth mentioning that the fact that the parameters r_λ can be obtained by the fit, makes this channel rather interesting. Other channels such as $B^0 \to D^{*\mp}\pi^{\pm}$ do not share this feature, and the parameter r (only one in this case) has to be supplied externally [14].

4.2 Event Generation

As stated in the previous Section, we use the EvtGen event generator. A configuration file that holds all the settings one wishes EvtGen to use, is passed to the generator.

A sample configuration file from this study is included in the Appendix as there are some very important differences when using EvtGen with '`SVV_NONCPEIGEN`' model with respect to other models. Moreover we have found the EvtGen manual severely lacking in this regard. Hence, we believe the interested reader can benefit from the elaboration and a practical example on the use of the said model.

The main difference between '`SVV_NONCPEIGEN`' and the majority of other models is, that mixing is already included in the model. Ordinarily one would use the '`VSS_BMIX`' model to decay the $\Upsilon(4S)$ particle into a pair of $B^0, \bar{B}^0$ mesons in a way which includes the mixing effects. When using the '`SVV_NONCPEIGEN`' one has to decay the $\Upsilon(4S)$ using a simple '`VSS`' model that gets just the kinematics right. Then, *only* the B^0 meson has to be passed to the '`SVV_NONCPEIGEN`', which decides if it really decayed as a B^0 or whether it has oscillated into a $\bar{B}^0$ first.

The reason why only B^0 can be passed to the '`SVV_NONCPEIGEN`' is prosaic: the EvtGen authors have not yet finished coding the $\bar{B}^0$ decay. EvtGen's manual notes, that this will be fixed 'later'.

The second difference from other models is that because of a bug in the code one has to input $2\phi_1 + \phi_3 + \pi$ as the weak phase, e.g., by leaving ϕ_1 intact and adding π to ϕ_3, as we have done in the provided sample configuration file.

Detailed analysis regarding the bug can be found in Section 5.2.

4.3 Extraction of Observables

EvtGen outputs produced events as tables, each representing one event. The table consists of a list of all involved particles, every one with a defined mother and daughters, if applicable, as well as four-momentum and space-time coordinates of its creation (in the laboratory frame).

We start by obtaining the time difference between the B meson decays from the creation times of their daughters, converted to the B mesons' proper time.

Next, we transform all the particles, using boosts and rotations, into the 'pseudo-frame' depicted in Figure 3.1. Please take note it is not an actual observational reference frame as the 'a' and 'b' sides were transformed differently. Once this is done, retrieving the angle observables is a simple matter of getting some of the particles' polar angles.

As we work on the generator level, the decay type can be easily inferred from the particles present in the decay chain.

4.4 Fitters

For fitting, we utilize the RooFit data modeling toolkit [23], originally developed for BaBar, now widely used in other experiments as well. The Minuit minimization engine [24] handles the actual minimization.

We created two fitters. The first being time-independent, employing *both* time integrated distributions (3.42) and (3.60), with the user being able to choose which one to use. This fitter retrieves the three helicity or transversity amplitudes using an unbinned maximum likelihood fit.

The second fitter is time-dependent, working in a much larger parameter space, designed to recover the 11 parameters listed in Section 4.1. It uses a simultaneous unbinned maximum likelihood fit to the four decay types.

Chapter 5

Results

5.1 Time-Independent Results

As mentioned in the previous Chapter, the time-independent fitter is able to work with both helicity and transversity distributions. During some early testing the transversity version seemed to be more reliable (although the difference was not very significant), so we chose to use it instead of the helicity one.

We want to validate the fitter by comparing our estimated fit uncertainties to that of the CLEO collaboration, which conducted the measurement with ~ 600 events [25]. It is worth mentioning that CLEO had very small background and thus it is reasonable to compare our results with theirs, even though we do not have a background at all.

As the values reported by CLEO are expressed in the helicity basis, we opt to report the input values and results in the helicity basis as well, to make comparison easier. The fitter converts them internally to the transversity basis and back as needed.

After settling on a type of distribution to use, we want to make sure the fitter is stable with respect to initial values of the helicity amplitudes. To verify that, we generate a sample file of 600 events and run the fitter on it 720 times, with different initial values - a so called 'scan of the parameter space'. The scanned volume of the parameter space can be seen in Table 5.1. Please note that we exclude unphysical starting values, such as $\sum_\lambda |H_\lambda|^2 > 1$ and use the constraints mentioned in Section 4.1, i.e., $\sum_\lambda |H_\lambda|^2 = 1$ and $\arg(H_0) \equiv 0$. The sample data

quantity	from	to	step	steps
$\lvert H_+\rvert$	0.00	0.40	0.10	5
$\arg(H_+)$	0.70	2.10	0.15	10
$\lvert H_0\rvert$	0.85	1.00	0.10	2
$\arg(H_-)$	0.00	1.05	0.15	8

Table 5.1: Scanned volume of the parameter space

quantity	μ	σ_{stat}	σ_{sys}
$\lvert H_+\rvert$	0.107	0.031	0.011
$\arg(H_+)$	1.42	0.27	0.04
$\lvert H_0\rvert$	0.941	0.009	0.006
$\arg(H_0)$		$\equiv 0$	
$\lvert H_-\rvert$	0.322	0.025	0.016
$\arg(H_-)$	0.31	0.12	0.04

Table 5.2: Helicity amplitudes measured by CLEO

set is generated using the amplitudes measured by the CLEO collaboration; they are given in Table 5.2.

The fitter exhibits remarkable stability as only 2 of the 720 fits failed to recover the correct parameters. This was due to a variable reaching its limit, where the numeric minimization engine got stuck. A variable equal to its limit value is a so obviously incorrect result, that we do not believe this could be a problem when attempting to assess a fit to real-world data. There do not seem to be any mirror solutions or shallow minima in the likelihood function, that could cause problems.

Another technique commonly employed to test fitters is a 'toy Monte Carlo study'. It is used to determine the bias a fitter might have. Furthermore, in many analyses it is very difficult or even impossible to estimate uncertainties analyticaly as the measurement is a result of a complicated procedure, often involving multiple simultaneous fits, each depending on a number of unknown parameters. A toy Monte Carlo study can recover uncertainties' estimates in such a case.

The idea is to create a simplified model of the measurement and run the

pseudo-experiment many times, each with a different random number seed. The width of the distribution of the measured values can be taken as the estimate of the measurement uncertainty.

Our toy Monte Carlo study comprises of a 1000 pseudo-experiments, each with 600 events. Distributions of the obtained central values, fit uncertainties and pulls, are depicted in Figures 5.1, 5.2 and 5.3, respectively. In our case the standard deviations of the amplitude distributions are almost equal to the mean of their respective error distributions, hinting that the errors recovered by the fit are reasonable.

Another way to test the reliability of the statistical error calculated for the fit and an estimation of a potential bias, is calculating the 'pull distribution'. A pull of a random variable x that is distributed as a gaussian with mean μ and standard deviation σ is defined as

$$p = \frac{x - \mu}{\sigma}. \tag{5.1}$$

It is apparent that after generating the random value x many times, p will be distributed as a gaussian with mean 0 and standard deviation of 1. Thanks to the central limit theorem this simple property can be applied to a wide range of situations.

By taking a fit result τ_{fit} with an uncertainty σ_{fit} and a true, generator, value τ_{gen} we can check if

$$p = \frac{\tau_{\text{fit}} - \tau_{\text{gen}}}{\sigma_{\text{fit}}} \tag{5.2}$$

is distributed as the above-mentioned gaussian with mean 0 and standard deviation of 1.

Means of the central values and the uncertainties for the amplitudes as well as for the pulls were collated into Table 5.3. The central values obtained by the toy Monte Carlo study are well within 1σ of the true, generator, values. The uncertainties are almost identical to the CLEO statistical uncertainties. Moreover, the pull distributions are consistent with a unit-width gaussian, indicating that the obtained fit uncertainties are reliable.

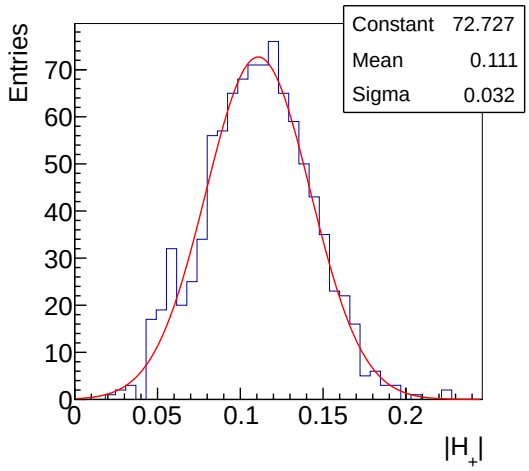

(a) Distribution of fitted $|H_+|$

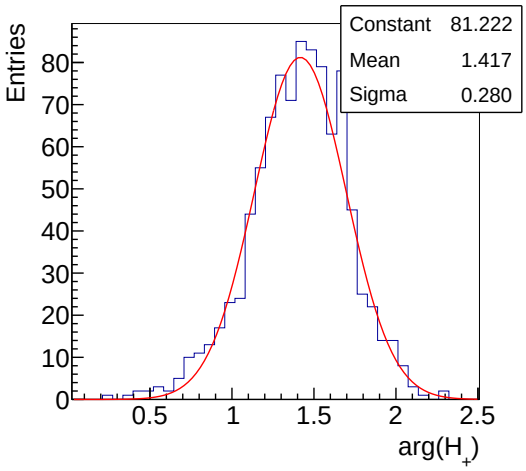

(b) Distribution of fitted $\arg(H_+)$

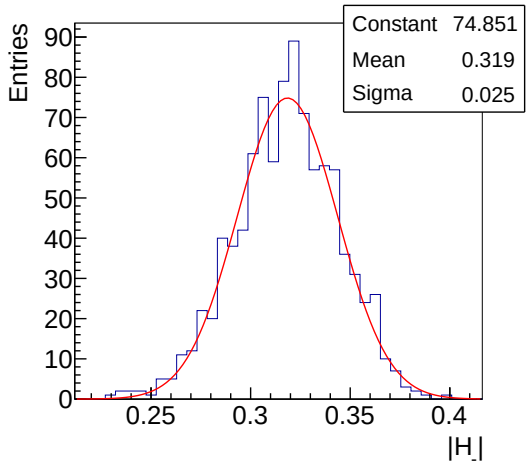

(c) Distribution of fitted $|H_-|$

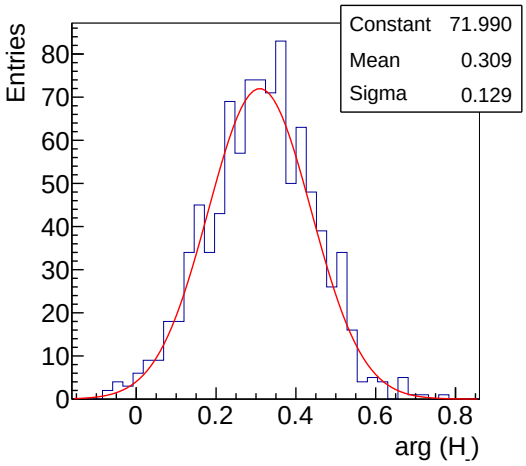

(d) Distribution of fitted $\arg(H_-)$

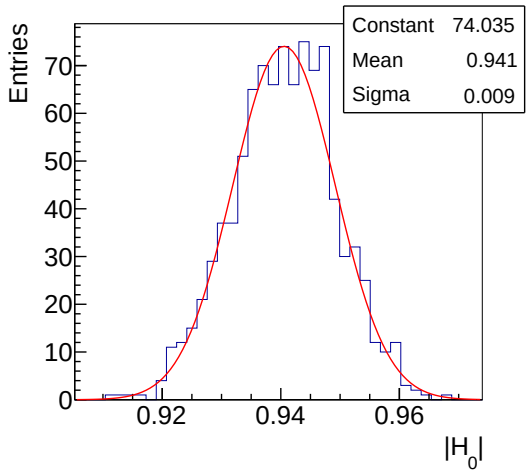

(e) Distribution of fitted $|H_0|$

Figure 5.1: Distributions of the fitted helicity amplitudes

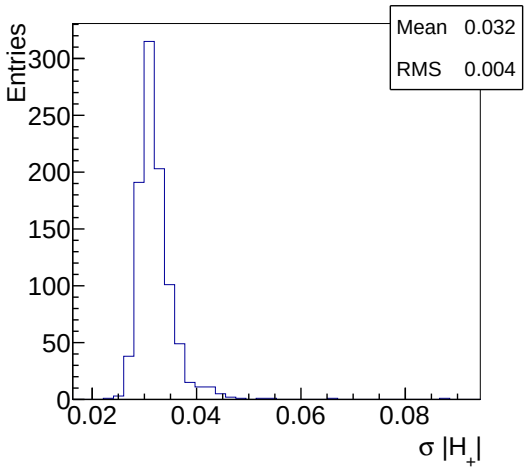

(a) Error distribution of fitted $|H_+|$

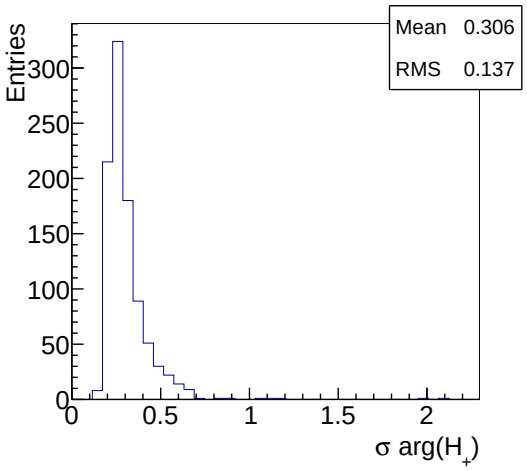

(b) Error distribution of fitted $\arg(H_+)$

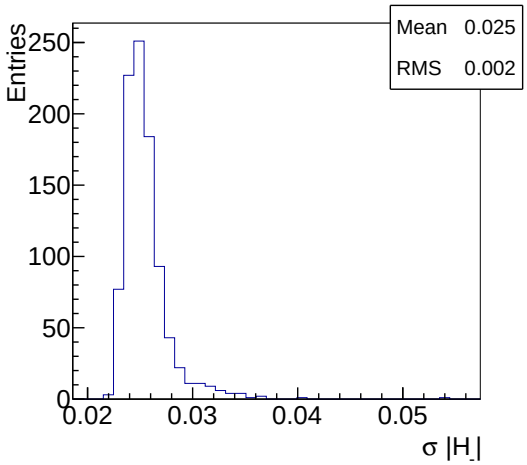

(c) Error distribution of fitted $|H_-|$

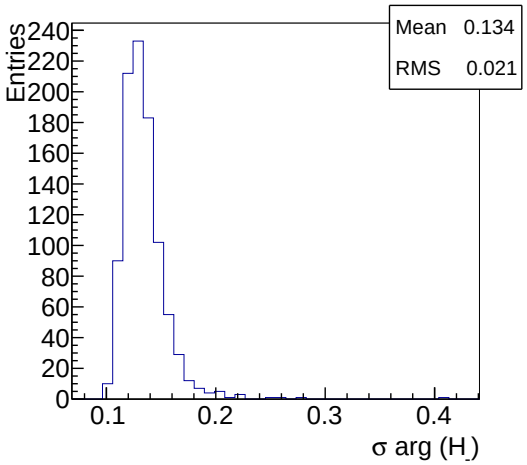

(d) Error distribution of fitted $\arg(H_-)$

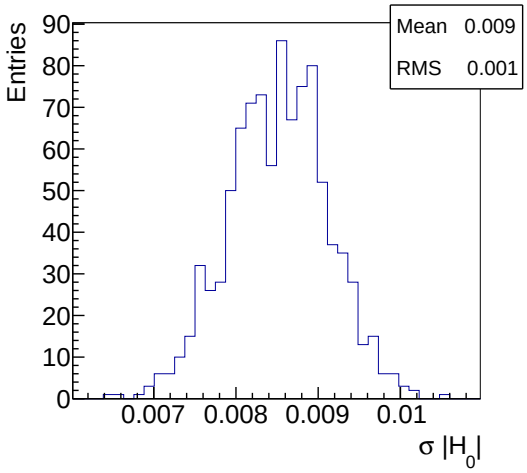

(e) Error distribution of fitted $|H_0|$

Figure 5.2: Error distributions of the fitted helicity amplitudes

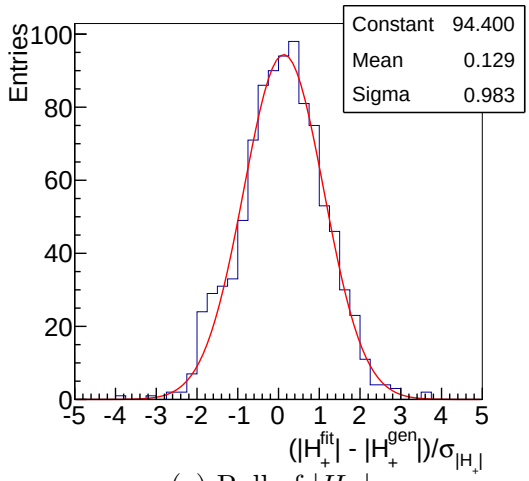

(a) Pull of $|H_+|$

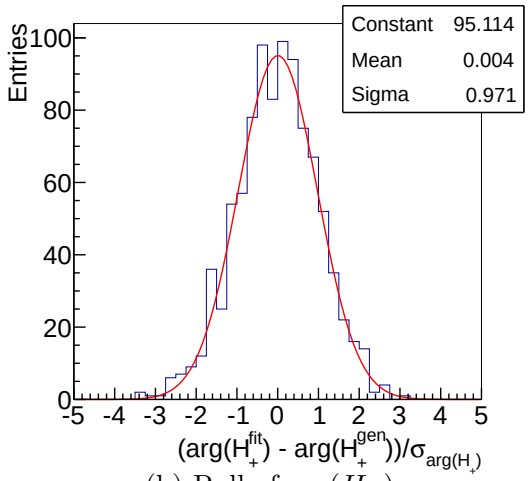

(b) Pull of $\arg(H_+)$

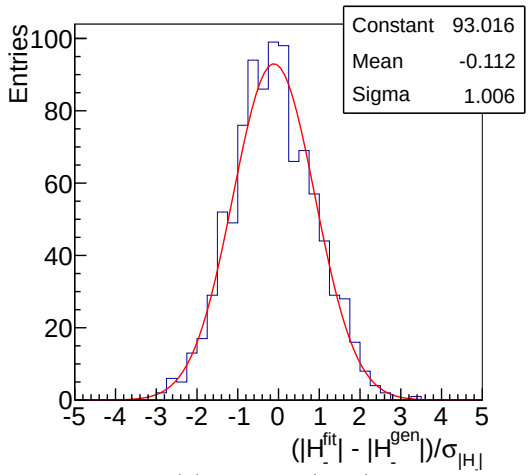

(c) Pull of $|H_-|$

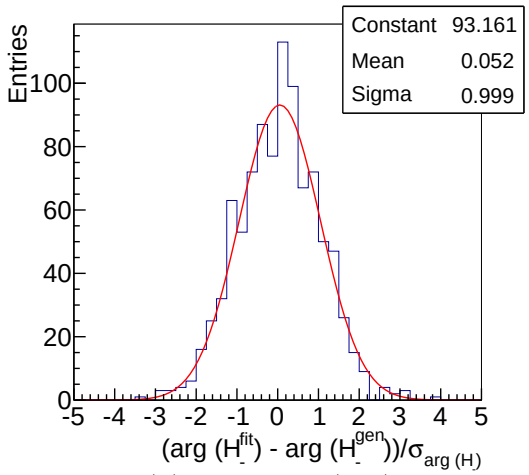

(d) Pull of $\arg(H_-)$

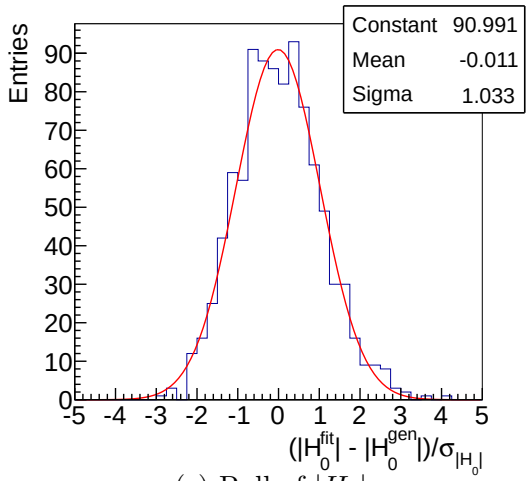

(e) Pull of $|H_0|$

Figure 5.3: Pull plots of the helicity amplitudes

quantity	amplitudes		pulls	
	μ	σ	μ	σ
$\lvert H_+\rvert$	0.111	0.032	0.128	0.978
$\arg(H_+)$	1.42	0.31	-0.005	0.979
$\lvert H_0\rvert$	0.941	0.009	-0.013	1.027
$\lvert H_-\rvert$	0.319	0.025	-0.112	1.007
$\arg(H_-)$	0.31	0.13	0.046	1.012

Table 5.3: Collated results of the toy Monte Carlo study

5.2 Time-Dependent Results

The time-dependent angular measurement of $B^0 \to D^{*\mp}\rho^{\pm}$ has not been carried out by anyone yet, so we do not have any preceding results to compare to. A paper from 2000 [26] proposes this channel as a viable means to measure $\sin(2\phi_1 + \phi_3)$ in the first-generation B-factories. The authors estimate that roughly $\sim 10^8$ $B\bar{B}$ pairs in total, would be required for this measurement.

The Belle experiment has accumulated a total integrated luminosity of $\mathcal{L}_{\text{total}} = 771\,\text{fb}^{-1}$ when running on $\Upsilon(4S)$ energy [27]. This translates to 7.71×10^8 $B\bar{B}$ pairs, and thus a time-depentent measurement is plausible according to the paper's authors.

To estimate the number of actual $B^0 \to D^*\rho$ decays that could be extracted from Belle data, we turn to a previous paper by Belle regarding $B^0 \to D^*\pi$ decays [28]. This study recovered ~ 31500 signal events, using a $\mathcal{L}_{\text{BN833}} = 350\,\text{fb}^{-1}$ data set. The branching fractions of the $D^*\pi$ and our $D^*\rho$ channels according to PDG are [8]:

$$\begin{aligned} \mathcal{B}_{D^{*-}\pi^+} &= 2.76 \times 10^{-3}, \\ \mathcal{B}_{D^{*-}\rho^+} &= 6.8 \times 10^{-3}. \end{aligned} \tag{5.3}$$

We expect a smaller efficiency in our channel because of a π^0 in the decay chain; a rough estimate could be $\epsilon = 0.65$ of the $D^*\pi$ channel. This leads to an expected

type	$\lvert p_+\rvert$	$\arg p_+$	$\lvert p_0\rvert$	$\arg p_0$	$\lvert p_-\rvert$	$\arg p_-$
favored	0.107	1.42	0.941	0	0.322	0.31
suppressed	0.00107	1.42	0.00941	0	0.00322	0.31

Table 5.4: SVV_NONCPEIGEN amplitude input values

number of signal events

$$N^{\text{sig}}_{D^{*-}\rho^+} = N^{\text{sig}}_{D^{*-}\pi^+} \frac{\mathcal{L}_{\text{total}}}{\mathcal{L}_{\text{BN833}}} \frac{\mathcal{B}_{D^{*-}\rho^+}}{\mathcal{B}_{D^{*-}\pi^+}} \epsilon \approx 10^5. \tag{5.4}$$

This high statistic together with the fact that the fit does not need externally supplied parameters such as r_λ, makes this channel very interesting.

For testing purposes, we generate a sample data set containing 10^5 events using the `SVV_NONCPEIGEN` model. The supplied amplitude input values are listed in Table 5.4.

Apart from these, we have also supplied:

- Δm_d - the difference of mass between the two B meson mass eigenstates; introduced in equation (3.77)
- ϕ_1 and ϕ_3 - the angles of the unitarity triangle defined in equation (3.99)

The values of these parameters are the ones used by Belle to create generic Monte Carlo data (retrieved from the official Belle EvtGen generic decay configuration file):

$$\Delta m_d = 0.502 \times 10^{12}\,\text{s}^{-1}, \qquad \phi_1 = 0.3800, \qquad \phi_3 = 1.0337. \tag{5.5}$$

Note, that in Table 5.4, we have intentionally labeled the amplitudes p_λ instead of H_λ to stress the important difference between them. Delving into EvtGen code, one discovers that

$$p^{\text{fav}}_\lambda = |a_m| e^{i \arg(F_{cm})}, \qquad p^{\text{sup}}_\lambda = |\bar{b}_m| e^{i \arg(\bar{F}_{um})}, \tag{5.6}$$

from which we can infer the following expressions for our parameters of choice

$$r_\lambda = \frac{p^{\text{sup}}_\lambda}{p^{\text{fav}}_\lambda}, \qquad \delta_\lambda = \arg(p^{\text{sup}}_\lambda) - \arg(p^{\text{fav}}_\lambda). \tag{5.7}$$

λ	$\lvert H_\lambda \rvert$	$\arg H_\lambda$	r_λ	δ_λ
+	0.107	1.42	0.01	0
0	0.941	0	0.01	0
-	0.322	0.31	0.01	0

Table 5.5: The translated SVV_NONCPEIGEN input values

The EvtGen model `SVV_NONCPEIGEN` can be given either 12 or 24 amplitude input values. When only 12 of these parameters are specified (as in our case), EvtGen assumes no direct CP violation and sets

$$|a_m|e^{i\arg(F_{cm})} = |\bar{a}_m|e^{i\arg(\bar{F}_{cm})}, \qquad |\bar{b}_m|e^{i\arg(\bar{F}_{um})} = |b_m|e^{i\arg(F_{um})}. \tag{5.8}$$

Rigorously, this is not true; however, only the ratios of suppressed to favoured parameters appear in the final angular distribution, therefore the individual terms are irrelevant, as long as the ratios are correct. Indeed, relations (3.94) ensure that the ratio of the left hand sides of equations (5.8) is equal to the ratio of the right hand sides.

The result of translating the values from Table 5.4 into the parameters we introduced in Chapter 3 can be seen in Table 5.5.

The values of δ_λ are chosen arbitrarily for the initial tests as we have no prior knowledge of what their real values might be. In Chapter 3 we explained how one can use the CKM matrix elements' magnitudes to make an estimate of the parameters r_λ. The estimate is very roughly $\frac{1}{60}$, but we are being conservative by rounding it to $\frac{1}{100}$. Take note that the smaller r_λ are, the more difficult it is to extract the CP violation parameters.

Starting work on the time-dependent fitter, we soon encountered trouble with the time distributions of the 4 modes. After disabling the fitting function, fixing all the parameters to the true, generator, values and just plotting the probability distribution functions (PDFs) onto the data, the discrepancy is still present.

The real problem is not easily discovered, because for some strong phase values, e.g., $\delta_\lambda = 0$, it appears as if one has simply switched the B^0 and $\bar{B}^0$ decays; see Figure 5.4. Together with the very non-standard `SVV_NONCPEIGEN`'s approach to mixing, as mentioned in Section 4.2, that changes how the decay

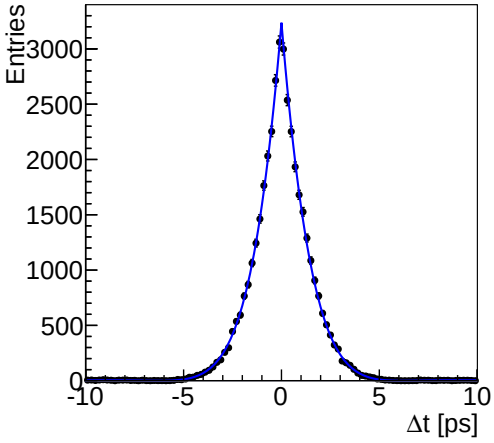

(a) Time distribution of $B^0 \to D^{*-}\rho^+$

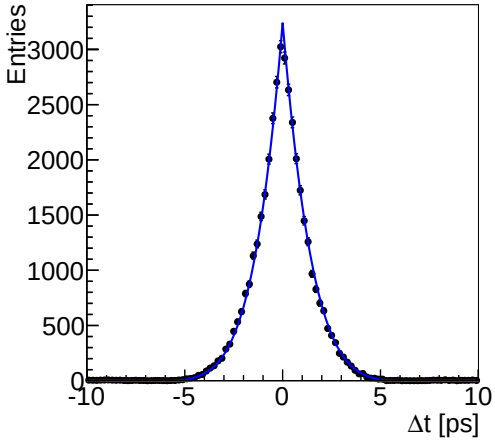

(b) Time distribution of $\bar{B}^0 \to D^{*+}\rho^-$

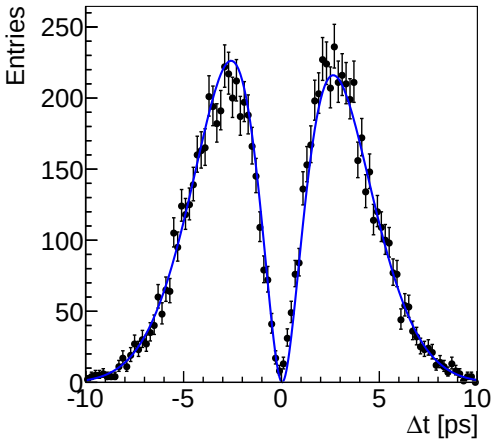

(c) Time distribution of $B^0 \to D^{*+}\rho^-$

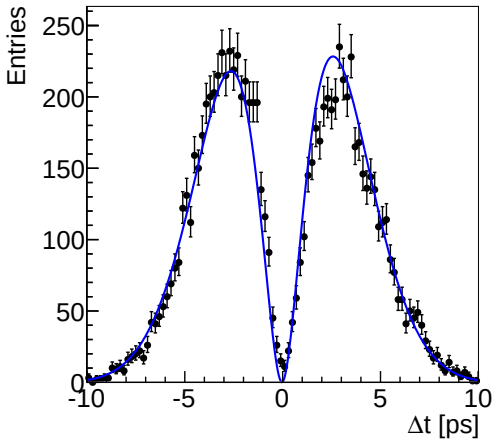

(d) Time distribution of $\bar{B}^0 \to D^{*-}\rho^+$

Figure 5.4: Time distributions with incorrect EvtGen data

type has to be inferred from the generated particles, it is tempting to conclude that the algorithm one uses to retrieve decay types returns them switched.

However, introducing a non-zero strong phase breaks the mirror symmetry between B^0 and $\bar{B}^0$ decays and can thus help us figure out if it indeed is a confusion of decay types. Generating a sample data set with

$$r_\lambda = 0.1, \quad \lambda \in \{+, 0, -\}, \qquad \delta_0 = 1.45, \tag{5.9}$$

all the other values staying the same as in Table 5.5, makes the discrepancy easily observable by eye and we see that switching decay types does not solve the problem; inspect Figure 5.5.

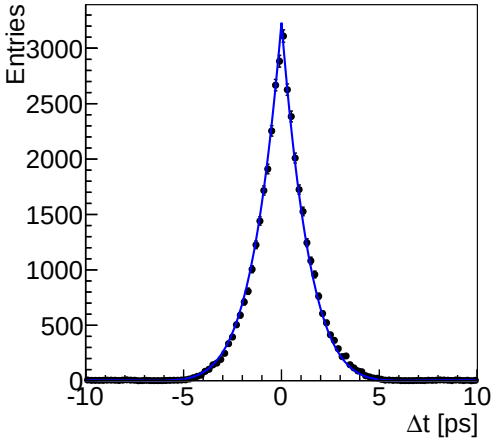

(a) Time distribution of $B^0 \to D^{*-}\rho^+$

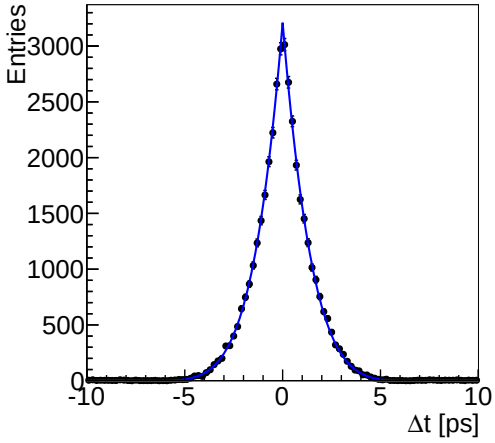

(b) Time distribution of $\bar{B}^0 \to D^{*+}\rho^-$

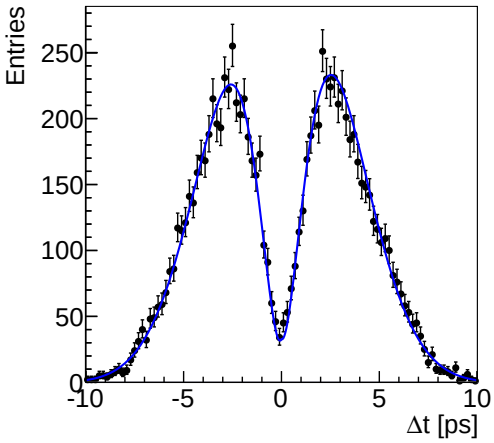

(c) Time distribution of $B^0 \to D^{*+}\rho^-$

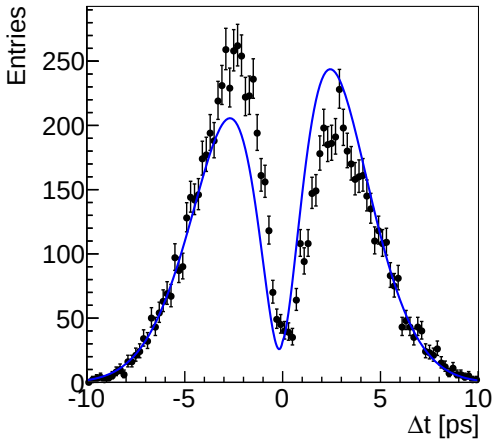

(d) Time distribution of $\bar{B}^0 \to D^{*-}\rho^+$

Figure 5.5: Time distributions with incorrect EvtGen data; $r_\lambda = 0.1, \delta_0 = 1.45$

After making sure the problem was not in our fitter, we identified the real culprit: EvtGen. In the `SVV_NONCPEIGEN` model code one can find that the pure flavor $B(t)$ states are given as

$$\begin{aligned} |B^0(t)\rangle &= e^{-\frac{\gamma}{2}t}\left(|B^0\rangle \cos\frac{\Delta m_d\, t}{2} + \frac{q}{p}|\bar{B}^0\rangle i \sin\frac{\Delta m_d\, t}{2}\right), \\ |\bar{B}^0(t)\rangle &= e^{-\frac{\gamma}{2}t}\left(|\bar{B}^0\rangle \cos\frac{\Delta m_d\, t}{2} + \frac{p}{q}|B^0\rangle i \sin\frac{\Delta m_d\, t}{2}\right). \end{aligned} \tag{5.10}$$

Take note of the switched sign with respect to (3.79). This sign is definition-dependent as it can be absorbed into the $\frac{q}{p}$ factor or into the phase difference between $|B^0\rangle$ and $|\bar{B}^0\rangle$. However EvtGen uses the same conventions as we do

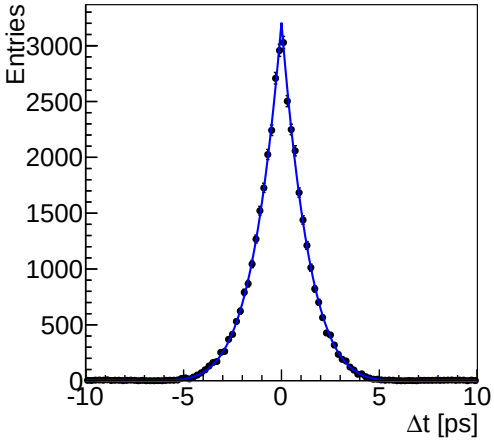

(a) Time distribution of $B^0 \to D^{*-}\rho^+$

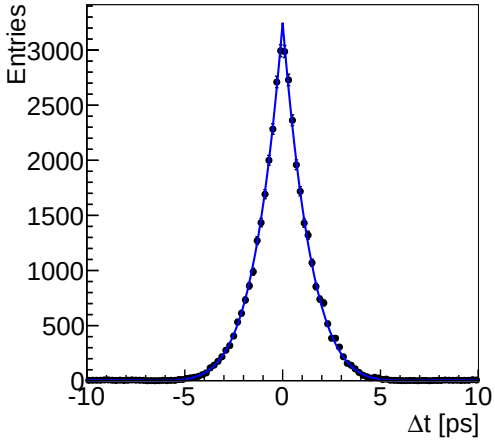

(b) Time distribution of $\bar{B}^0 \to D^{*+}\rho^-$

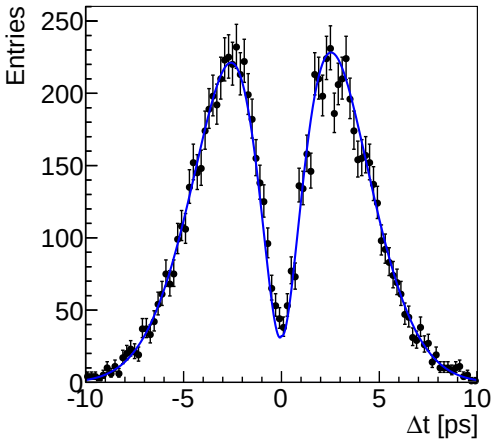

(c) Time distribution of $B^0 \to D^{*+}\rho^-$

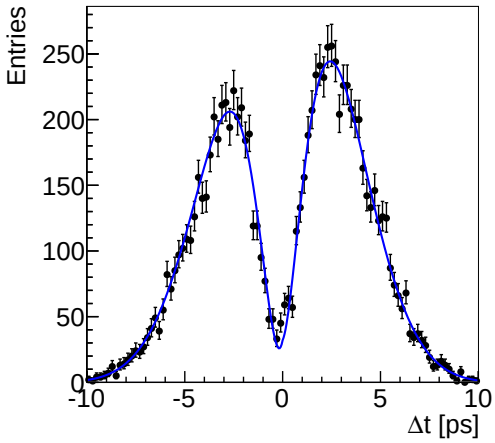

(d) Time distribution of $\bar{B}^0 \to D^{*-}\rho^+$

Figure 5.6: Time distributions with correct EvtGen data; $r_\lambda = 0.1, \delta_0 = 1.45$

and therefore uses wrong PDFs to generate the decays.

Fortunately this problem can be easily remedied even without modifying and recompiling EvtGen, simply by supplying altered weak angles. Looking at equations (3.96) we see that by changing the signs of ρ_m and $\bar{\rho}_m$ we can counterbalance the wrong sign. Perhaps the easiest way of doing that is by changing $\phi_3 \to \phi_3 + \pi$ in the EvtGen input file. Carrying out this substitution and generating the data set again fixes the problem as can be seen in Figure 5.6.

Moving on, we fit the data generated by EvtGen using the values from Table 5.5 (with the correction described above). Unfortunately the recovered results are incorrect. The recovered amplitudes are reasonable, the r_λ, δ_λ and the weak phase are, however, not.

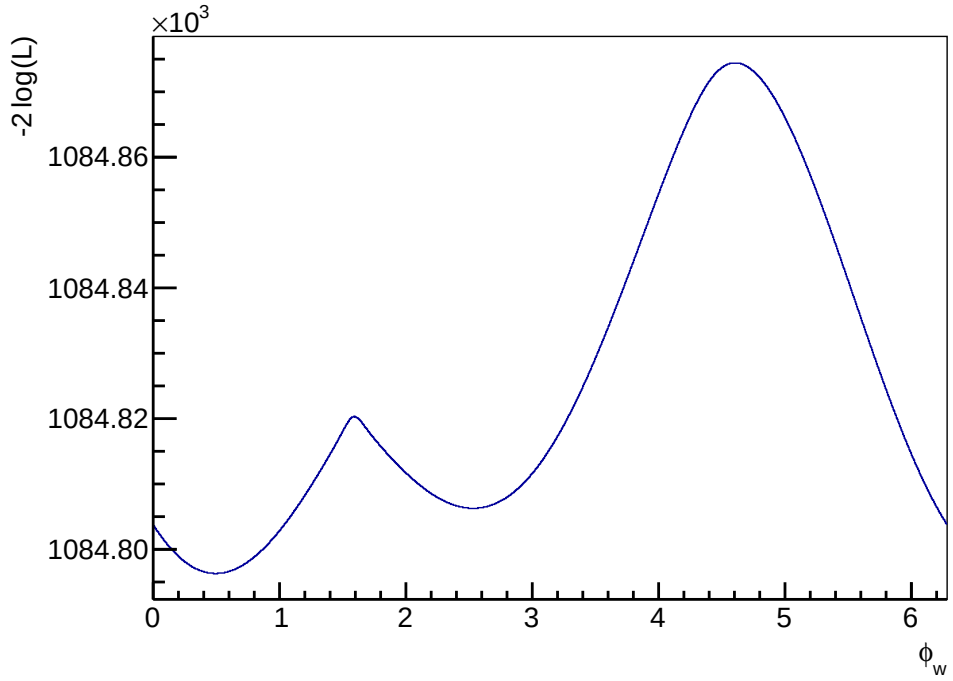

Figure 5.7: Plot of the log-likelihood function with respect to the weak phase

We fix all the parameters except the weak phase ϕ_w to exclude numeric difficulties stemming from correlation, etc., thus fitting a function of a single parameter. Still, the fit returns either

$$\phi_w^{\text{fit}} = 2.50 \pm 0.15 \tag{5.11}$$

or

$$\phi_w^{\text{fit}} = 0.60 \pm 0.14 \tag{5.12}$$

depending on the initial values, instead of the generator value $\phi_w^{\text{gen}} = 1.79$. We check the log-likelihood function for shallow minima and other possible causes of this behavior. It exhibits no such features as evidenced by a scan of the log-likelihood function depicted in Figure 5.7.

Unfortunately, the time-frame of this thesis did not permit us to continue the search for the source of this problem. However, I plan to continue studying this channel during my doctoral studies, and hopefully, if the sensitivity study results are favorable, conduct the complete measurement.

Conclusion

We have studied the plausibility of using the Belle experiment data set to extract the Standard Model CP violation parameters, e.g., $\sin(2\phi_1 + \phi_3)$, through the $B^0 \to D^{*\mp}\rho^{\pm}$ channel. This particular channel is very interesting because it is quite self-sufficient; one does not have to externally supply some of the parameters such as the ratios of the suppressed to the favored decay amplitudes as in many other studies.

Two fitters have been created a time-independent and a time-dependent one. The time-independent fitter can be used to extract the helicity or transversity amplitudes associated with the decay. It exhibits great stability and reports gratifying fit uncertainties as testified by a comparison to a prior CLEO study as well as by pull distribution tests.

During the construction of the time-dependent fitter we have discovered a fault in the EvtGen event generator. The fault has been analysed and a temporary workaround has been proposed. Even after correcting this issue, the fitter fails to recover the correct values. The log-likelihood function has been studied to illuminate the source of the problem. It does not seem to be of a numerical precision nature, but rather something more fundamental.

Unfortunately the time-scope of this thesis did not allow us to pursue the matter further. Nevertheless, I plan to continue studying this channel during my doctoral studies and if the study concludes that the measurement is plausible, conduct the complete measurement.

Bibliography

[1] T. D. Lee and C. N. Yang. Question of Parity Conservation in Weak Interactions. *Phys. Rev.*, 104:254–258, October 1956.

[2] C. S. Wu et al. Experimental Test of Parity Conservation in Beta Decay. *Phys. Rev.*, 105:1413–1415, February 1957.

[3] Nobelprize.org. The Nobel Prize in Physics 1957. `http://www.nobelprize.org/nobel_prizes/physics/laureates/1957`. [Online; accessed 23 Jul. 2012].

[4] L. Landau. On the Conservation Laws for Weak Interactions. *Nuclear Physics*, 3(1):127–131, 1957.

[5] J. H. Christenson et al. Evidence for the 2π Decay of the K_2^0 Meson. *Phys. Rev. Lett.*, 13:138–140, July 1964.

[6] R. Aaij et al. Evidence for CP Violation in Time-Integrated $D^0 \to h^-h^+$ Decay Rates. *Phys. Rev. Lett.*, 108:111602, 2012.

[7] KEK. Institutions in Belle Collaboration. Belle Internal Memo, May 2012.

[8] J. Beringer et al. The Review of Particle Physics. *Phys. Rev. D*, 86(010001), 2012.

[9] KEK. Machine Parameters of the KEKB. `http://www-kekb.kek.jp/Commissioning/MachineParameters`, June 2009.

[10] A. Abashian et al. The Belle Detector. *Nucl. Instrum. Meth. A*, 479:117–232, 2002.

[11] T. Abe et al. Belle II Technical Design Report. *ArXiv e-prints*, November 2010.

[12] E. P. Wigner. *Group Theory and Its Application to the Quantum Mechanics of Atomic Spectra*. Academic Press, 1959.

[13] M. Jacob and G.C. Wick. On the General Theory of Collisions for Particles with Spin. *Annals of Physics*, 7(4):404 – 428, 1959.

[14] K. Abe, M. Satpathy, and H. Yamamoto. Time dependent angular analyses of B decays. 2001. Belle Note #419.

[15] M. L. Boas. *Mathematical Methods in the Physical Sciences*. Wiley, 2006.

[16] Belle and BaBar Collaborations. *Physics of the B-Factories*. 2012. Retrieved from `http://www.slac.stanford.edu/xorg/BFLB/` (Unpublished).

[17] V. Devanathan. *Angular Momentum Techniques in Quantum Mechanics*. Fundamental Theories of Physics. Springer, 1999.

[18] J. Hořejší. *Fundamentals Of Electroweak Theory*. Karolinum Press, 2003.

[19] M. Kobayashi and T. Maskawa. CP-Violation in the Renormalizable Theory of Weak Interaction. *Progr. Theoret. Phys.*, 49(2):652–657, 1973.

[20] A. Ryd et al. EvtGen A Monte Carlo Generator for B-Physics. *BAD*, 522 v6, February 2005.

[21] I. Adachi et al. Computing system for the Belle experiment. *eConf*, C0303241:MODT010, 2003.

[22] F. Rademakers and R. Brun. ROOT: An Object-Oriented Data Analysis Framework. *Linux Journal*, 51, July 1998.

[23] W. Verkerke and D. Kirkby. The RooFit Toolkit for Data Modeling. In L. Lyons and M. K. Ünel, editors, *Statistical Problems in Particle Physics, Astrophysics and Cosmology*, pages 186–190. Imperial College Press, 2006.

[24] F. James and M. Roos. MINUIT - A System for Function Minimization and Analysis of the Parameter Errors and Correlations. *Comput. Phys. Commun.*, 10(6):343–67, 1975.

[25] S. E. Csorna et al. Measurements of the branching fractions and helicity amplitudes in $B \to D^* \rho$ decays. *Phys. Rev.*, D67:112002, 2003.

[26] David London, Nita Sinha, and Rahul Sinha. Extracting weak phase information from $B \to V(1)V(2)$ decays. *Phys. Rev. Lett.*, 85:1807–1810, 2000.

[27] KEK. Integrated Luminosity of B-factories. `http://belle.kek.jp/bdocs/lumi_belle.png`. [Online; accessed 23 Jul. 2012].

[28] T. Sarangi. TCPV studies in $B \to D^{(*)}\pi$ decays with 350fb^{-1} data. 2006. Belle Note #833.

List of Tables

List of Figures

Appendix

```
# Decay table for B0->generic , B0Bar->D*+- + rho-+
#                 B0->D*+- + rho-+ , B0Bar->generic
#
#
#  July 21th

# This is gamma + pi. An EvtGen bug is accounted for by adding
# pi to 2*beta + gamma

Define dm 0.507e12
Define beta  0.3800
Define gammapluspi 4.1753


# Aliases for our particles, i.e., signal + definitions of
# charge-conjugated pairs

Alias MyB0   B0

Alias MyD*+ D*+
Alias MyD*- D*-
ChargeConj  MyD*+ MyD*-

Alias MyD0 D0
Alias MyD0Bar anti-D0
ChargeConj MyD0 MyD0Bar


# Y(4S) -> B0 B0Bar
#
# Decay model: VSS --> vector (with C=-1) to scalar+scalar
# with no mixing

Decay Upsilon(4S)
# brFr Decay products    Decay model
1.000  MyB0 anti-B0  VSS;
Enddecay
```

```
# B0->D* rho
#
# Decay model: SVV_NONCPEIGEN --> Scalar to vector+vector
# where final state is not CP eigenstate

Decay MyB0
# brFr  Decay products Decay model
1.000    MyD*- rho+   PHOTOS SVV_NONCPEIGEN dm beta gammapluspi
                           0.107   1.42 0.941   0 0.322   0.31
                           0.00107 1.42 0.00941 0 0.00322 0.31;
Enddecay


# D* -> D0 + pi

Decay MyD*+
# brFr  Decay products Decay model
1.000    MyD0 pi+    PHOTOS VSS;
Enddecay
CDecay MyD*-


# D0 -> K + pi

Decay MyD0
# brFr  Decay products Decay model
1.000    K- pi+    PHOTOS PHSP;
Enddecay
CDecay MyD0Bar

End
```